Journal of Materials Chemistry A

Nonfullerene acceptors for P3HT-based organic solar cells

Journal:	*Journal of Materials Chemistry A*
Manuscript ID	TA-REV-04-2021-003219.R1
Article Type:	Review Article
Date Submitted by the Author:	28-May-2021
Complete List of Authors:	Chatterjee, Shreyam; Osaka University, ISIR, Department of Soft Nanomaterials JINNAI, Seihou; Osaka University, Department of soft Nanomaterials Ie, Yutaka; Osaka University, The Institute of Scientific and Industrial Research

ARTICLE

Nonfullerene acceptors for P3HT-based organic solar cells

Shreyam Chatterjee,*[a] Seihou Jinnai[a] and Yutaka Ie*[a,b]

Received 00th January 20xx,
Accepted 00th January 20xx

DOI: 10.1039/x0xx00000x

Progressive advancement of remarkably high power conversion efficiencies (PCEs) of organic solar cells (OSCs) largely depends on the development of non-fullerene acceptors (NFAs), revealing the astonishing ability of OSCs to shift the paradigm of sustainable energy researches. Poly(3-hexylthiophene) (P3HT) is still positioned as a promising donor in cost-effectiveness and bulk availability. Recently, OSCs comprised of P3HT and newly designed NFAs reached over 10% PCE, which increased the expectation of the large-scale production of OSCs. In this review, we summarize the critical evolution of fundamental molecular design for various NFAs over the last decade, specifically for the combination with P3HT. Some important NFAs with new diversity in their building blocks and excellent performance are highlighted. We also summarize nonhalogenated green solvent processes for the P3HT:NFA-based OSCs. Brief introductions are also provided regarding the large-area fabrication. This review offers clear guidelines with a comprehensive view for further developing the NFAs compatible with P3HT-based OSCs for future commercialization.

Introduction:

Efforts to restrict global warming are closely related to the sustainable development goals, which aim to achieve environmental protection, social comfort, and economic prosperity. The ideal global circumstances can be achieved by reducing the consumption of fossil fuels and switching to environmentally friendly energy sources. Reducing energy-related CO_2 emissions is the key to the energy transition. In this regard, Si-based inorganic solar cells have been extensively utilized worldwide. However, these solar cells have faced some limitations such as high cost of material and manufacturing, low flexibility, heavyweight, and environmental destruction.[1,2]

Organic solar cells (OSCs) have evolved as promising next-generation energy sources due to the advantages such as low cost, flexibility, lightness, high-throughput process, large-area production, and printing processes (Fig. 1).[3,4] The active layers of OSCs are typically composed of a p-type semiconductor (electron donor) and an n-type semiconductor (electron acceptor). The resulting donor:acceptor (D:A) blend forms interpenetrating bulk-heterojunction (BHJ) structures in the films, which can overcome small exciton diffusion length of ~10 nm of organic materials and thus maximize the D–A interfacial area for efficient photoinduced charge separation.[5-7] Although high power conversion efficiencies (PCEs) over 18%[8-11] and lifespan of up to 10 years[12–15] were reported, innovation efforts for social implementation are still insufficient due to the difficulty of fabricating OSCs suitable for their applications.

Since the 1990s, when the effectiveness of fullerene (C_{60}) and [6,6]-phenyl-C_x-butyric acid methyl ester (PC_xBM: x = 61 or 71) was verified,[16,17] fullerene derivatives have been utilized as standard acceptor materials in OSC studies. Regioregular poly(3-hexylthiophene) (P3HT) has been utilized as a representative donor material. However, as a narrow optical bandgap to broaden the absorption range of solar light is essential to increase PCEs, D–A type narrow bandgap copolymers have positioned as high-performance donor materials with fullerene-based acceptors.

Fig. 1 (Left) P3HT-based OSCs on a flexible substrate. (Right) Evaluation of long-term stablity of OSCs on the top of roof. Reproduced with the permission from ideal star inc.

Considerable efforts have been directed to establish the fundamental structure-property relationships that control the performance of these polymer:fullerene systems within the device. Fullerene acceptors have large electron affinity, high electron-mobility, delocalization of the lowest unoccupied molecular orbital (LUMO), isotropic electron transport, formation of domains with appropriate length-scale for charge separation, and reversible multiple electrochemical reductions to yield stable reduced charged species.[18-22] Despite these advantages, they have faced some serious limitations such as (i) low absorption in the visible spectrum, (ii) inadequate scope for synthesis to control the structural tunability of energy levels, (iii) high cost, (iv) morphological instability in the blend films, and (iv) macroscopic crystalline-structure formation.[23,24]

To overcome these limitations of fullerene-based acceptors, electron-accepting small π-conjugated molecules, oligomers,

[a] The Institute of Scientific and Industrial Research (ISIR), Osaka University, 8-1 Mihogaoka, Ibaraki, Osaka 567-0047, Japan
E-mail: shreyam@sanken.osaka-u.ac.jp
[b] Innovative Catalysis Science Division, Institute for Open and Transdisciplinary Research Initiatives (OTRI), Osaka University

and polymers, termed as nonfullerene acceptors (NFAs), have been studied.[25,26] NFAs can design from various π-conjugated building units and assemble through direct synthetic protocols, and their purifications are easily performed by conventional methods. In terms of molecular properties, NFAs have large extinction coefficients in the ultraviolet-visible (UV-vis) region, providing acceptor domains with complementary light harvesting (to their respective donor components). Additionally, the NFAs-based OSCs provide a remarkable low energetic offset for generation of free charge carriers, which improve the overall performance of OSCs by low voltage loss with enhanced device stability.[27-29] Considering the significant progress in the development of NFAs, particularly after the emergence of "Y-series" of NFAs within the last five years,[30] PCEs based on D–A type donor and NFAs have been approaching 18%. Thus, a constructive review of NFAs compatible with P3HT is also urgently needed to guide researchers toward further improvement of P3HT:NFA-based OSCs, as P3HT-based OSCs still have advantages for social implementation, as discussed below.

1. Working principle of OSCs:

A typical solar cell device converts incident photons from sunlight into electrical current. The working principle of the device includes four key steps: (i) light absorption by the active layer and generation of Coulombically tightly-bound excitons; (ii) diffusion of the excitons to the D–A interfaces, (iii) exciton dissociation at the interfaces. First, charge transfer (CT) states are created, which in sequence fully dissociate into free holes and electrons (charge carriers); and (iv) charges drift through the separate donor and acceptor domains, where holes and electrons are finally collected at the anode and cathode electrodes, respectively (Fig. 2(a)). Each of the processes is vital and can be decisive in the overall solar cell performance. Here, the energy difference between the LUMO energy level of the acceptor and the highest occupied molecular orbital (HOMO) energy level of the donor provides the primary driving force for charge separation and is directly related to the photovoltage (open-circuit voltage, V_{OC}). Two types of exciton dissociation can occur after the photo irradiation in OSCs: (1) the donor is photoexcited, and then the excited electron is transferred to the acceptor (Channel-I); (2) the acceptor is photoexcited followed by the hole transfer from acceptor to P3HT (Channel-II) (Fig. 2(b)). The utilization of both types of carrier generation further improves the OSC performance.

When we focus on the OSC device architecture, work functions of both bottom and top electrodes can be tuned by using different interfacial layers. Thus, insertion of proper interfacial layers alters the charge extraction efficiency by adequately matching the Fermi levels of either donor or acceptor in the BHJ for the hole or electron collection, respectively. Depending on this mechanism, two types of device structures of the OSCs can be fabricated: (i) conventional and (ii) inverted structures, in which the electrode polarity is reversed in direction (Fig. 2(c)).[31] In the conventional OSCs, a p-doped conducting polymer, (poly(3,4-ethylenedioxythiophene:poly(styrene sulfonate) (PEDOT:PSS), is commonly used to modify indium tin oxide (ITO) electrodes to improve hole extraction, and low work function metals such as LiF/Al or Ca/Al are often used in the top as a cathode to ensure effective electron extraction. As the low work function metal is vulnerable to oxidation under ambient conditions, the resulting degradation of electrode becomes a major problem for OSCs with conventional structure. Here, to enhance the stability of the OSC devices, inverted structure is useful, where TiO_2 or ZnO is prepared on ITO electrodes, and high work function metal (more air-stable) is used on the top as an anode for hole collection. Thus, inverted OSCs have superior ambient stability and better compatibility to all solution roll-to-roll (R2R) processing due to the metal anode deposition as colloidal solution (e.g., Ag nanoparticles) .[32]

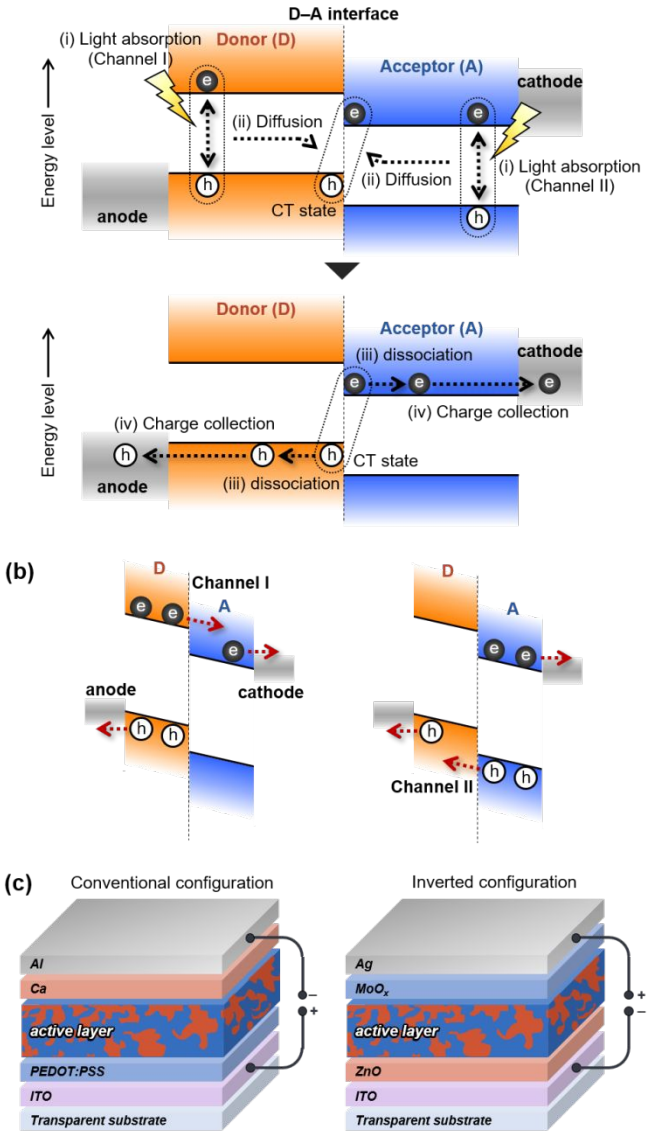

Fig. 2 (a) Device operating mechanism of OSCs. (b) Mechanism of photocurrent generation via different (channels I and II) exciton dissociation pathways in OSCs. (c) Cartoon models of (left) conventional and (right) inverted OSCs.

2. Why P3HT-based OSCs are important?

P3HT has been extensively used for donor materials in organic electronic devices due to chemical and electrochemical stability, and appropriate HOMO energy level of approximately -4.9 eV (Fig. 3(a)).[33-35] Furthermore, the high crystallinity of P3HT enables the formation of aligned molecular configurations in the solid state, leading to high hole mobility (Fig. 3(b)).[34]

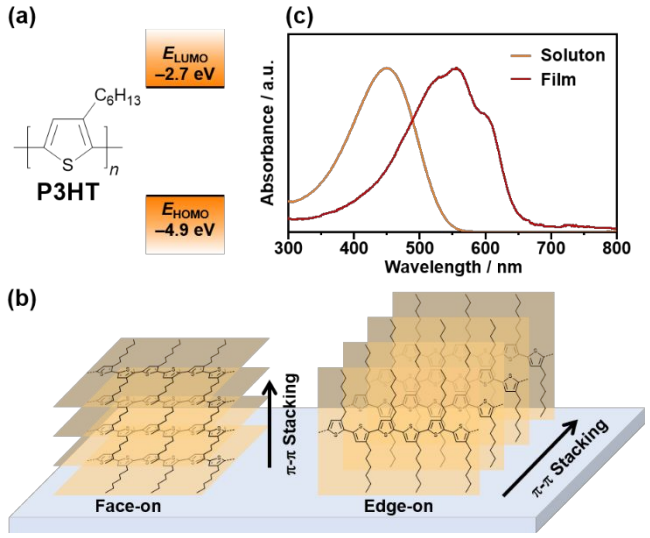

Fig. 3 (a) Chemical structure of P3HT and its frontier energy levels relative to the vacuum level. (b) Normalized UV-vis absorption spectra of P3HT in solution and thin film. (b) Schematic illustration of the face-on and edge-on configurations of P3HT.

Thus, P3HT has been one of the most investigated donor polymers in OSC studies. In particular, the P3HT:PC_xBM-based OSCs were regarded as the standard for a long time and have assisted to clarify many fundamental issues, guiding OSC research directions.[36-39] In the P3HT:PC_xBM system, P3HT acts as the key light-harvesting, and its absorption is within 300–600 nm (Fig. 3(c)). Thus, the intrinsic narrow absorption range for the P3HT:PCBM system led to the development of medium or low bandgap D–A type polymers such as polythieno[3,4-*b*]-thiophene-alt-benzodithiophene (PTB7-Th) and poly[(2,6-(4,8-bis(5-(2-ethylhexyl)thiophen-2-yl)-benzo[1,2-*b*:4,5-*b*']dithiophene))-alt-(5,5-(1',3'-di-2-thienyl-5',7'-bis(2-ethylhexyl)benzo[1',2'-*c*:4',5'-*c*']dithiophene-4,8-dione)] (PBDB-T). Although the pairing of NFAs with these narrow bandgap D–A type polymers has yielded PCEs of 16–18%,[10,11,40-42] the sophisticated chemical structures of these polymers results in low large-scale viability, low batch-to-batch reproducibility, and high synthetic cost. Furthermore, high-performance NFAs have also faced the same problems. Thus, the combination of D–A type polymers with NFAs becomes a considerable obstacle for their practical application.

P3HT consists of 3-hexylthiophene as the repeating monomer unit. As the established synthetic routes are easy,[43,44] P3HT can be obtained at a low cost (425.7 $/g) compared to typical D–A type polymers (PTB7-Th: 2333.8 $/g; PBDB-T: 1471.3 $/g).[45] Moreover, P3HT has been synthesized in flow with excellent control over the molecular weight (M_w), polydispersity index (PDI), and regioregularity.[46] Indeed, P3HT is currently one of the few polymers available in bulk quantities,[41] being a feasible candidate donor for the commercialization of OSCs. Its use in large-area R2R printed solar cells has been widely demonstrated.[47-51] Thus, P3HT is positioned to be the exclusive donor for large-scale manufactured OSCs.

It is to be noted that a myriad of polythiophene derivative such as (poly[5,5'- bis(2-butyloctyl)-(2,2'-bithiophene)-4,4'-dicarboxylate-*alt*-5,5'-2,2'-bithiophene] (PDCBT) was developed for OSC application.[52,53] Although the cost of PDCBT (4340 $/g) is still high compared to P3HT, these polythiophene derivatives have great potentials for practical application. For further details of polythophene derivatives see the reviews.[54-56]

3. Small molecule NFAs in P3HT-based OSCs:

3.1. NDI-based NFAs:

Naphthalene 1,8:4,5-tetracarboxylic diimide (NDI) has characteristic physical and electronic properties such as high electron affinity, high electron mobility, strong absorption coefficient, and thermal stability. Another advantage of the NDI unit is the capacity to tune its solubility via incorporating lipophilic alkyl chains on the nitrogen atoms.[57] This alkyl chain is also important in generating unique molecular alignments in the thin films.[58] In contrast, aggregation behaviour, wide energy gap, and narrow light absorption range beyond 400 nm hinder the use of pristine NDA as NFAs. Therefore, chemical modification of NDI-based NFAs has been extensively performed (Fig. 4, Table 1).

Note that the HOMO and LUMO values in this review were taken from the original papers. Since these values were estimated using various techniques, we suggest that the values should be compared with caution. The PCEs in this review showed the maximum values in the original papers. We unify the solvent abbreviation as follows: DCM for dichloromethane, THF for tetrahyrdofuran, CF for chloroform, CB for chlorobenzene, and *o*-DCB for *o*-dichlorobenzene.

In 2011, Jenekhe et al. reported NDI-based NFAs named as **NDI-3TH**, where terthiophene units flanked the central NDI moiety.[59] This chemical modification enabled the obtainment of optical bandgaps in the 1.4–2.1 eV range, relatively low LUMO energy level of -4.0 eV, and HOMO energy level between -5.5 and -6.1 eV. The highest PCE of 1.5% was observed for P3HT:**NDI-3TH**-based OSCs (Fig 5(a)(b)). IThis study was one of the first that concluded that additives (1,8-diiodooctane (DIO)) are effective to significant increase in the PCEs in the NFAs-based OSCs (Fig. 5(c)(d)). Bright-field transmission electron microscopy (BF-TEM) images of the blend films without DIO showed well-mixed, bicontinuous, percolated morphologies, with P3HT nanowires evenly dispersed in the **NDI-3TH** (Fig. 5(c)). The DIO-added films formed interconnected, well-woven pathways for charge transport, whereas P3HT domains remained in the nanowire network (Fig. 5(d)). To explore a set of criteria for the design of NFAs, the homologous series of NDI-based NFAs with different oligothiophene cores, **NDI-*n*TH** (*n* = 1-4) and **NDI-*n*T** (*n* = 2, 3), were developed.[60] All these molecules showed ambipolar characteristics of hole (μ_h) and electron (μ_e) transport in organic field-effect transistors

(OFETs). For P3HT-based OSCs, photovoltaic responses were observed when μ_e/μ_h >1, and the formation of bicontinuous nanoscale morphologies in the blend film is also essential for a high PCE.

The combination of electron-donating core substituents with the electron-accepting NDI framework can create a push-pull system. A series of NDI derivatives with amino core substituents and aromatic substituents on the nitrogen atoms was synthesized.[61,62] Although these molecules showed limited PCEs of less than 1%, relatively high V_{oc} values were obtained due to the high LUMO energy levels of the amino core-substituted NDI framework.

A NDI-based NFA (**NDI-N1**) having naphthalene imide at end groups was synthesized by Bhosale et al. [63] The OSCs using this molecule showed a PCE of 2.91%. The additional introduction of a thiophene linker (**NDI-N2**) further increased the PCE to 4.04%. The smooth morphologies of the blend films indicated the better intermixing of P3HT and **NDI-N2**, which resulted in the high device performance. The researchers further developed **N3** and **N4** based on an A–A'–A design, where A' is NDI and A is rhodanine or 1,3-indandione.[64] The basic A–A'–A design dictates superior flexibility in optimizing energy levels to match with P3HT simply by the choice of the A group. OSCs using **N3** and **N4** showed PCEs of 4.76 and 3.52%, respectively. This research supports that the studied A–A'–A design has a strong potential to develop a series of high-performing NFAs. In fact, Bhosale et al. developed a unique NDI-based NFA **N10**, which is composed of NDI as both central and terminal functionalities. This molecule showed a PCE of 7.65%,[65] which is the highest for P3HT:NDI-based NFAs to date.

Recently, Rao et al. demonstrated the successful use of an A–A1–D–A type modular format to synthesize V-shaped NFAs.[66] The new acceptor **NDICz-6**, which is comprised of an electron-rich carbazole D core, NDI A core together with tetracyanoquinodimethane as A1 unit, was synthesized. The P3HT:**NDICz-6**-based device exhibited the highest PCE of 7.58%. Interestingly, after solvent vapour annealing using carbon disulphide, an increase of PCE of approximately two-fold was obtained compared to that of as-cast blend films.

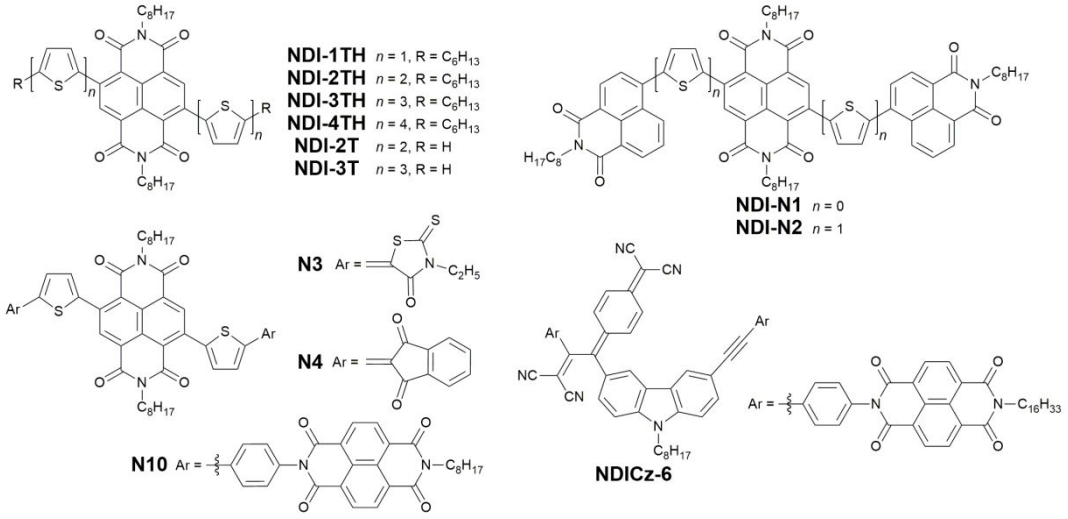

Fig. 4 Chemical structures of NDI-based NFAs.

Table 1. Properties, photovoltaic characteristics, and blend film properties of NDI-based NFAs

Acceptor	LUMO /eV	HOMO /eV	E_g /eV	D:A ratio	Process solvent	V_{oc} /V	J_{sc} /mA cm^{-2}	FF	PCE /%	μ_e [a] /cm^2 V^{-1}s^{-1}	μ_h [a] /cm^2 V^{-1}s^{-1}	Ref
NDI-3TH	−4.10	−5.50	1.40	1:1	DCM	0.82	3.51	0.52	**1.50**	NR	NR	59
NDI-N1	−3.69	−5.95	2.26	1:1	*o*-DCB	0.84	6.13	0.56	**2.91**	NR	NR	63
NDI-N2	−4.10	−5.86	1.76	1:1	*o*-DCB	0.81	8.58	0.58	**4.04**	NR	NR	63
N3	−3.90	−5.87	1.97	1:1.2	*o*-DCB	0.87	8.87	0.60	**4.62**	2.98 x 10^{-3}	NR	64
N4	−3.89	−6.05	2.16	1:1.2	*o*-DCB	0.91	6.69	0.58	**3.52**	1.83 x 10^{-3}	NR	64
N10	−4.15	−5.70	1.55	1:1.2	*o*-DCB	0.99	12.08	0.64	**7.65**	NR	NR	65
NDICz-6	−4.19	−5.91	1.72	1:1.5	CF	0.94	13.67	0.59	**7.58**	10^{-3}	NR	66

a) Blend film.

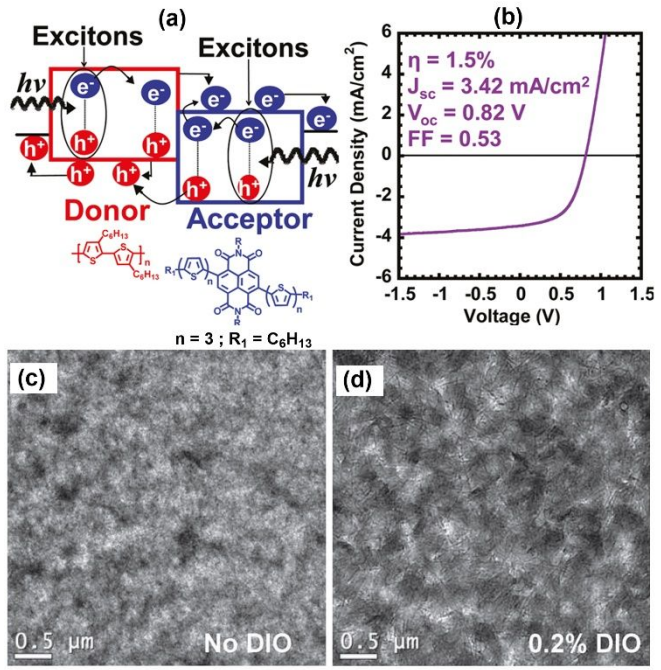

Fig. 5 (a) Schematic picture of charge generation and separation for P3HT:**NDI-*n*TH**. (b) *J-V* curve of P3HT:**NDI-3TH**-based OSCs. Reproduced with the permission from ref 60. Copyright 2011, American Chemical Society. (c,d) BF-TEM images of the P3HT:**NDI-3TH** (1:1 wt/wt) blend films containing different DIO concentrations. Reproduced with the permission from ref 59. Copyright 2011, John Wiley & Son.

3.2. PDI-based NFAs:

Among various rylene diimides, terrylene-3,4:11,12-tetracarboxylic diimide (PDI) has been the main material to construct NFAs owing to its capability of being functionalized into solution-processable derivatives with nanoscale structures maintaining high electron mobility and strong absorption coefficient. However, most PDI-based NFAs have bandgaps lower than 1.9 eV, and thus narrow bandgap D–A type donor polymers are generally suitable to complement the absorption. The recent advances in PDI-based NFAs for D–A type donor polymers have been published in several reviews.[67,68] For this reason, a limited number of PDI-based NFAs compatible to P3HT has been reported, as summarized below (Fig. 6, Table 2).

In 2012, Sharma et al. reported a symmetrical PDI derivative (**PBI**) bearing 2-(4-nitrophenyl)acrylonitrile group at the 1,7-bay position of the PDI framework.[69] **PBI** had an optical bandgap of 1.72 eV and a LUMO energy level of -3.9 eV. Under optimized condition using DIO as an additive and thermal treatment, the P3HT:**PBI** blend films showed balanced charge transport due to the enhanced crystallinity and increased hole mobility, resulting in a high PCE of up to 3.17%.

A series of PDI dimers bearing several arylene linkers was developed as NFAs, from which PCEs of up to 2.35% were achieved with PDI dimers having spirobifluorene linkers (**1**).[70] The utilization of three-dimensional (3D) structures such as tetraphenylmethane framework and silsesquioxane have been also effective for PDI-based OSCs.[71] These results indicate that non-planar 3D structures effectively suppress self-aggregation and crystallization of the PDI units, which is favourable for the improvement of solar cell performance. We summarize other NFAs bearing 3D structure in Section 3.8.

Yao et al. designed PDI-based NFAs having twisting chemical structures and amphiphilic nature.[72-74] **Bis-PDI-T-di-EG** having 2-methoxylethoxyl (EG) groups at the outer bay-regions of the dimeric backbone resulted in the highest PCE of 1.54% when 1-chloronaphthalene (CN) was used as a solvent additive. The molecular solvophobicity, which was generated by the EG groups at the bay-region, is considerably important in the photovoltaic characteristics.[72] Further tuning in the central unit by a conformationally-twisted 4,8-bis(2-(2-ethylhexylthienyl)) benzodithiophene (BDT-T) resulted in the BDT-T-bridged PDI dimer **2** and BDT-O-bridged PDI dimer **3**.[73] Due to the presence of 2-ethylhexylthienyl group in the central BDT-T unit, **2** exhibited a highly twisted conformation through steric pairing and π–π stacking to reduce the over aggregation tendency in the blend (Fig. 7). This distorted structure also helped **2** to achieve an excellent solution processability. In contrast, **3** showed an over-strong aggregation ability and very poor solution-processability, which hindered the fabrication of the device. When blended with the P3HT, the dimer **2** gave a PCE of 1.95% due to its excellent processability.

The swap of inner BDT-T and outer PDI units is also effective for NFAs: the PDI-based compound (**B-PDI-B**) showed a PCE of 1.7% by functionalizing the bay-region using the BDT-T units.[74]

Zhan et al. developed a twisted dimeric PDI (**IDT-2PDI**) with a bulky fused-ring indaceno[1,2-*b*:5,6-*b*']dithiophene (IDT) as a bridge.[75] The P3HT:**IDT-2PDI** blend film showed relatively balanced hole and electron mobilities of 10^{-4} cm^2 V^{-1} s^{-1} order, and thus this film showed a PCE of 2.61%.

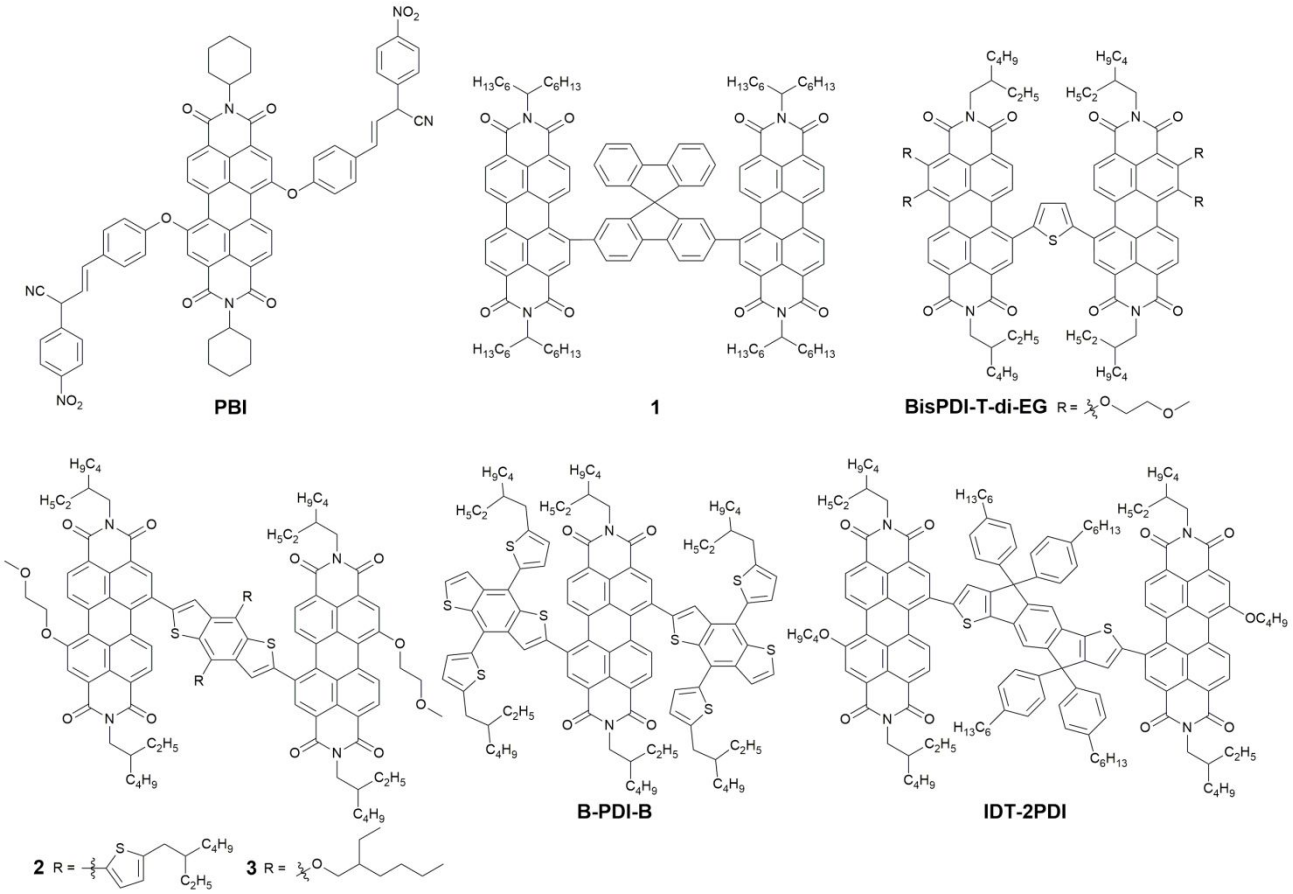

Fig. 6 Chemical structures of PDI-based NFAs.

Table 2. Properties, photovoltaic characteristics, and blend film properties of PDI-based NFAs

Acceptor	LUMO /eV	HOMO /eV	E_g /eV	D:A ratio	Process solvent	V_{oc} /V	J_{sc} /mA cm^{-2}	FF	PCE /%	μ_e [a] /cm^2 V^{-1}s^{-1}	μ_h [a] /cm^2 V^{-1}s^{-1}	Ref
PBI	−3.60	−5.80	2.20	1:1	THF[b]	0.78	7.40	0.55	**3.17**	5.6 x 10^{-4}	1.5 x 10^{-4}	69
1	−3.71	−5.71	1.62	1:1	*o*-DCB	0.61	5.92	0.65	**2.35**	7.1 x 10^{-5}	NR	70
Bis-PDI-T-di-EG	−3.84	−5.57	1.81	1:1	*o*-DCB[c]	0.67	3.83	0.60	**1.54**	5.4 x 10^{-4}	9.8 x 10^{-2}	72
2	−3.84	−5.48	1.64	1:2.2	*o*-DCB	0.68	5.83	0.49	**1.95**	3.4 x 10^{-4}	4.2 x 10^{-2}	73
B-PDI-B	−3.95	−5.57	1.62	1:2	*o*-DCB	0.61	5.3	0.51	**1.66**	1.96 x 10^{-5}	NR	74
IDT-2PDI	−3.83	−5.53	1.70	1:1	*o*-DCB	0.70	5.58	0.67	**2.61**	3.9 x 10^{-4}	7.5 x 10^{-4}	75
PMI-F-PMI	−3.54	−5.74	2.05	1:1	*o*-DCB	0.98	5.61	0.42	**2.30**	9.85 x 10^{-5}	1.29 x 10^{-3}	76
FFI-1	−3.48	−6.08	2.60	1:2	*o*-DCB	0.76	4.40	0.56	**1.86**	NR	NR	77
Th-PhCHO	−3.41	NR	NR	1:2	*o*-DCB	1.03	5.14	0.45	**2.40**	NR	NR	78
AFI3	−3.52	−5.99	2.47	1:2	*o*-DCB	0.96	5.21	0.47	**2.37**	NR	NR	79
DTI-4a	−3.61	−5.81	2.20	1:1	*o*-DCB[d]	0.61	4.31	0.55	**1.45**	NR	NR	81
Cor-NI	−3.24	NR	3.04			0.82	2.75	0.46	**1.03**	1.32 x 10^{-4}	NR	82

a) Blend film. Blend film including b) 1.5% of DIO, c) 1.75% of CN, d) 2.0% of CN.

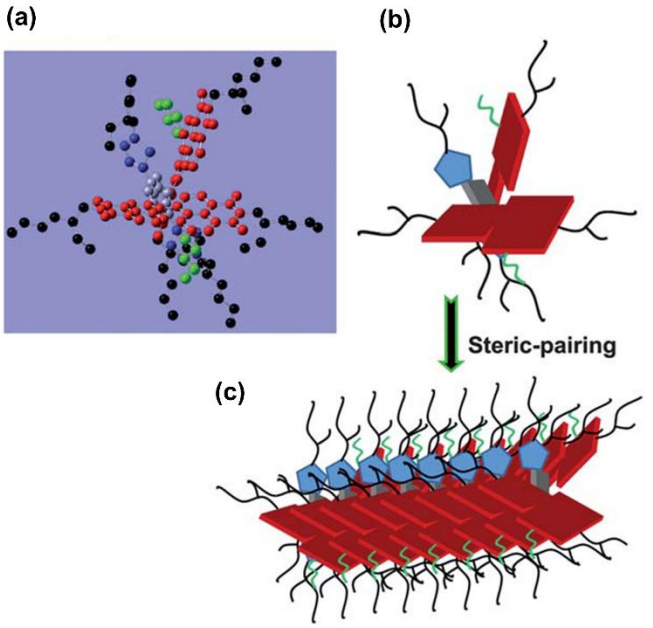

Fig. 7 (a) Optimal conformation of **2**, viewing along the 4,8-direction of the BDT unit. Note that, in this model, the PDI backbone is red labelled, the BDT unit is grey coloured, the thienyl units are blue coloured, the 2-methoxyethyl (EG) is green coloured and the 2-ethylhexyl (EH) tails are black. (b and c) Molecular packing models of dimer **2** under the direction of the steric-pairing effects. Reproduced with the permission from ref 73. Copyright 2013, The Royal Society of Chemistry.

3.3. Other rylene imide-based NFAs:

Other electron-accepting small molecules bearing rylene imide were also developed as small NFAs for P3HT-based OSCs (Fig. 8, Table 2). A fluorene-centered perylene monoimide dimer (**PMI-F-PMI**) with a partially non-coplanar configuration was developed.[76] The optimum PCE of the OSC based on **PMI-F-PMI** and P3HT increased to 2.30% due to the relatively balanced electron–hole transport and the smooth morphologies.

Pei et al. developed a series of fluoranthene-fused imide (**FFI-1**, **Th-PhCHO, Th-COOMe**) for NFAs.[77,78] Slow evaporation of the solvent and subsequent thermal annealing of the P3HT:**FFI-1** films resulted in an optimal grain size and uniform phase separation, with a PCE of 1.86%.[77] Subsequently, it was reported that the introduction of the bulky *p*-formylphenyl group was effective to improve the PCE up to 2.40% due to the improved molecular packing in the blend.[78] The extension of the π-conjugation was designed to adjust the charge-transporting properties and a series of acenaphtho fluoranthene-fused diimide derivatives (**AFI1**, **AFI2**, and **AFI3**) was synthesized. Inverted OSCs based on P3HT and **AFI3** achieved PCEs up to 2.37%.[79]

Wudl et al. established a facile and efficient synthetic route towards decacyclene triimide (**DTI-4a**). This molecule contains three naphthalene monoimide rings positioned in a three-fold symmetric pattern around a central benzene ring.[80,81] The electron affinity of this π-conjugated framework was increased by the presence of multiple electron-accepting imide moiety, thereby facilitating electron injection, and charge transport in the device. OSCs were fabricated using P3HT and **DTI-4a**, which exhibited a PCE of 1.6% and a fill factor of 0.57.

Cao et al. reported **Cor-PI** and **Cor-NI** as NFAs, which attached an electron-accepting phthalimide (PI) or naphthalimide (NI) unit to the corannulene core.[82] In these molecules, *N*-hexyl substituents were chosen to ensure sufficient solubility and film forming properties of the compounds. The large dihedral angle between the corannulene core and imide moieties of **Cor-PI** and **Cor-NI** improved the miscibility with P3HT, and the P3HT:**Cor-NI** blend film exhibited a PCE of up to 1.03%.

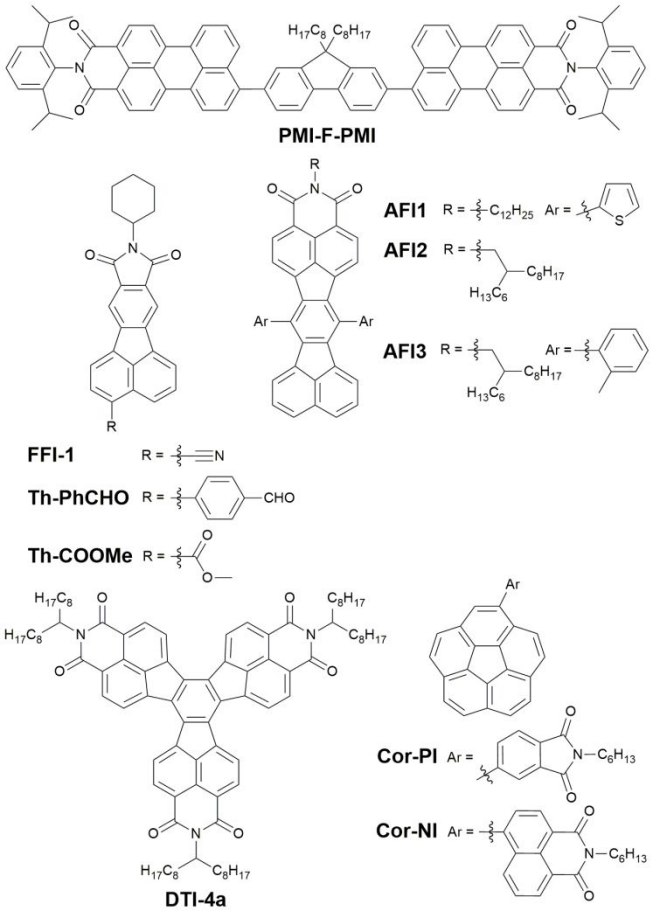

Fig. 8 Chemical structures of rylene imide-based NFAs.

3.4 NFAs with a three-membered conjugated unit in core:

In this section, we summarize representative NFAs bearing a three-membered conjugated unit in the central part (Fig. 9, Table 3). In most cases, the combination of central unit with characteristic terminal unit is critical for obtaining good PCEs. One of the effective terminal unit, 2,3-dihydro-1*H*-indene-1,3-dione (ID), was developed by Winzenberg et al.[83] They utilized fluorene and thiophene as well-established privileged structural templates and synthesized the electron-accepting molecule **FEHIDT**, which showed a PCE of 2.12%.

4,4-Difluoro-4-bora-3′,4′-diaza-*s*-indacene (BODIPY)-based small molecule (**BDP-CPDT**), which comprises a thiophene-based donor core and terminal BODIPY units conjugated through the *meso* position, was developed.[84] **BDP-CPDT**

showed a low-lying LUMO energy level of -3.79 eV and electron-transport characteristics in OFETs. This compound exhibited the highest PCE of 1.51% when CN was used as a solvent additive.

For the first time, NFAs having rhodanine dyes at the terminal unit were developed by Lim et al.[85] A small molecule acceptor (**Flu-RH**) showed a PCE of 3.08% with a high V_{oc} of 1.03 V. As summarized in this review, the use of rhodanine as the terminal unit contributes to NFAs performance.

Holliday et al. developed a revolutional NFA (**FBR**) comprised of 3-ethylrhodanine as a terminal unit.[86] The HOMO and LUMO energy levels of **FBR** were -5.70 and -3.57 eV, respectively. The HOMO of FBR was delocalized over the entire π-conjugated backbone, whereas the LUMO was concentrated onto the electron-deficient periphery (Fig. 10(a)). This LUMO distribution has advantages for efficient electron-transport along the neighbouring **FBR** molecules in the blend films. UV-vis absorption spectra showed that **FBR** can absorb in a considerably higher solar flux region of the spectrum compared to $PC_{61}BM$ (~300 nm), and the molar extinction coefficient of **FBR** was considerably higher than that of $PC_{61}BM$ (Fig. 10(b)). The nonplanar nature of **FBR** would act favourably to prevent the growth of large acceptor domains due to self-aggregation, and provide relatively isotropic charge transport (Fig. 10(c)). For the first time, OSCs based on **FBR** exceeded 4.0% PCE and outperformed $PC_{61}BM$-based cells (Fig. 10(d)). Additionally, the P3HT:**FBR** blend was highly intermixed, which substantially improved the morphological stability in the devices. Thus, **FBR** was one of the milestones in the P3HT:NFA-based OSC researches.

Diketopyrrolopyrrole (DPP)-attached molecule **$F(DPP)_2B_2$** showed HOMO and LUMO energy levels of -5.21 and -3.39 eV, respectively.[87] These energy levels were suitable for use as both a donor and an acceptor, and PCEs of more than 3.0% were obtained in both cases. In particular, a PCE of 3.17% was obtained when **$F(DPP)_2B_2$** was utilized as an NFA with P3HT. **F8-DPPTCN** was also developed, using fluorene as the core with arms of DPP having thiophene-2-carbonitrile as the terminal units.[88] This molecule had a LUMO energy level of -3.65 eV and a narrow bandgap of 1.66 eV. The P3HT:**F8-DPPTCN**-based OSCs showed a PCE of 2.37%.

A linear NFA (**DBS-2DPP**) using a dibenzosilole (DBS) as a core unit showed good nanoscale interpenetrating networks with long fibroid structure, which is beneficial to charge separation, and enhanced efficiency of OSC performance up to 2.05% PCE.[89]

A NFA named as **N7** was synthesized by using simple carbazole as central and DPP as terminal building blocks.[90] **N7** displayed a well-matched energy levels (HOMO = -5.56 eV and LUMO = -3.74 eV) with those of P3HT. OSCs based on **N7** showed a PCE of 2.30% with a high V_{OC} of 1.17 V.

NFAs based on 9-fluorenone or 9,10-anthraquinone as the central building block and DPP moieties as terminal groups, namely **DPP-FN-DPP** and **DPP-ANQ-DPP,** were developed.[91] Suboptimal morphologies with **DPP-ANQ-DPP** inhibited the crystallisation of P3HT chains, resulting in a PCE of 1.2%. NFAs bearing DPP in the central unit were also developed, and we summarize these structures in Section 3.7.

A2–A1–D–A1–A2-type NFAs **NAI-FN-NAI(BO)** were developed.[92] The OSCs based on P3HT:**NAI-FN-NAI(BO)** exhibited a PCE of 3.6%, which was attributed to the enhanced nanoscale morphologies of the active layer.

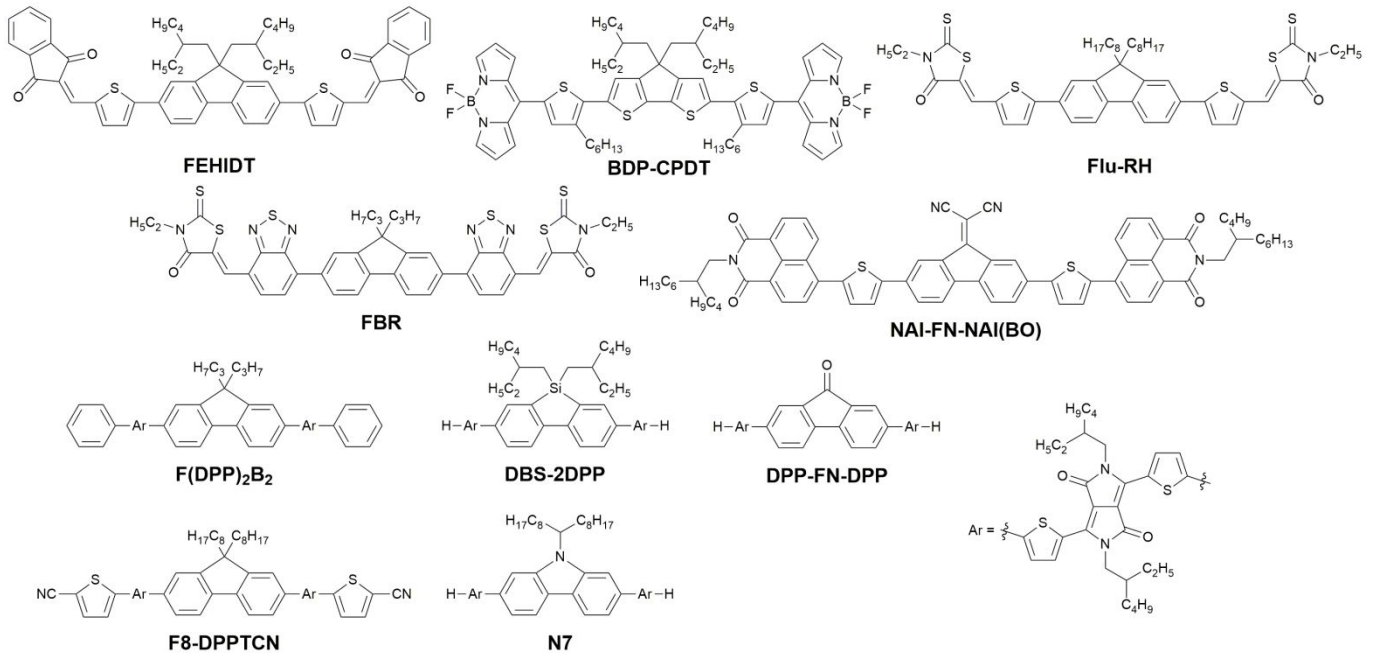

Fig. 9 Chemical structures of NFAs.

Table 3. Properties, photovoltaic characteristics, and blend film properties of NFAs with three-membered conjugated unit

Acceptor	LUMO /eV	HOMO /eV	E_g /eV	D:A ratio	Process solvent	V_{oc} /V	J_{sc} /mA cm^{-2}	FF	PCE /%	μ_e [a] /cm^2 V^{-1}s^{-1}	μ_h [a] /cm^2 V^{-1}s^{-1}	Ref
FEHIDT	−3.95	−5.95	2.00	1.2:1	*o*-DCB	0.95	3.82	0.67	**2.12**	NR	NR	83
BDP-CPDT	−3.82	−5.16	1.54	1:1.5	*o*-DCB	0.62	3.90	0.63	**1.51**	5.77 x 10^{-5}	NR	84
Flu-RH	−3.53	−5.58	2.05	1:1.5	*o*-DCB	1.03	5.70	0.52	**3.08**	NR	NR	85
FBR	−3.57	−5.70	2.14	1:1	CF:*o*-DCB (4:1)	0.82	7.95	0.63	**4.11**	2.6 x 10^{-5}	NR	86
F(DPP)$_2$B$_2$	−3.39	−5.21	1.82	1:1	CF	1.18	5.35	0.50	**3.17**	2.8 x 10^{-4}	4.3 x 10^{-5}	87
F8-DPPTCN	−3.65	−5.31	1.66	1:3	CF	0.97	6.25	0.39	**2.37**	1.12 x 10^{-3}	3.62 x 10^{-5}	88
DBS-2DPP	−3.28	−5.30	1.83	1.2:1	*o*-DCB	0.97	4.91	0.43	**2.05**	2.8 x 10^{-5}	6.1 x 10^{-4}	89
N7	−3.74	−5.56	1.82	1:1.2	*o*-DCB	1.17	3.16	0.62	**2.30**	NR	NR	90
DPP-FN-DPP	−3.81	−5.56	1.75	1:2	*o*-DCB	0.97	3.20	0.37	**1.2**	NR	NR	91
NAI-FN-NAI(BO)	−3.96	−6.07	2.11	1:1	CB	0.88	9.1	0.45	**3.6**	NR	NR	92

a) Blend film

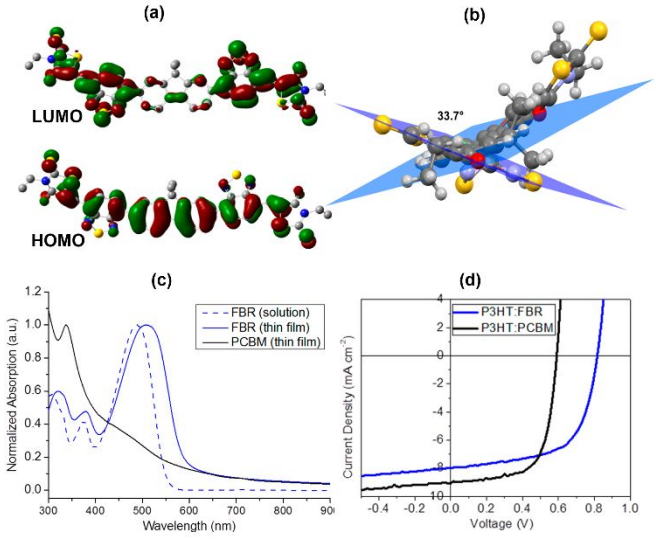

Fig. 10 (a) Optimized conformation of **FBR** calculated using Gaussian (B3LYP/6-31G*) to visualize the LUMO and HOMO distributions. (b) Normalized UV-vis absorption spectra of **FBR** in chloroform solution and thin film along with $PC_{61}BM$ films. (c) Dihedral planes of **FBR** from the minimum energy conformations calculated using Gaussian (B3LYP/6-31G*). (d) *J*–*V* curves of P3HT:**FBR** (blue) and P3HT:$PC_{61}BM$ (black) devices. Reproduced with the permission from ref 86. Copyright 2016, American Chemical Society.

3.5 NFAs with a five-membered conjugated unit in core:

In this section, we summarize recent mainstream NFAs that have a five-membered conjugated unit in the central part (Fig. 11, Table 4). A A–D–A-type NFA **IDT-2BR** based on indacenodithiophene (IDT) and rhodanine was designed by Zhan et al.[93] **IDT-2BR** adopts a rigid and coplanar backbone configuration, which facilitates charge transport. The peripheral substituents of hexylphenyl groups on the IDT moiety are beneficial for forming favourable interpenetrating networks without severe self-aggregation when mixing with P3HT. OSCs based on the P3HT:**IDT-2BR** films processed with 3% 1-chloronaphthalene as an additive achieved PCEs as high as 5.12%. This was the first report in which a PCE over 5% was obtained for a P3HT-based NFA.

IDT-based NFAs with NP as the end-capping group (**3**) were synthesised.[94] P3HT:**3**-based blend films showed a PCE up to 2.36%.

Holliday and McCulloch et al. have reported new acceptor derivatives (**O-IDTBR** and **EH-IDTBR**) to address the issues of spectral overlap and morphologies for **FBR**.[95] Useful chemical modifications, which include the replacement of the fluorene core with the IDT unit, led to the planarized molecular structure, and hence accomplished red-shift absorption and suitable crystallinity. **O-IDTBR** and **EH-IDTBR** showed high PCEs of 6.34 and 6.00%, respectively.

Baran and McCulloch et al. reported efficient and stable P3HT-based OSCs by utilizing a ternary approach; two NFAs were combined with P3HT for the active layer.[96] The replacement of the IDT core in **O-IDTBR**[95] with indacenodibenzene resulted in a new NFA (**IDFBR**), which increased the bandgap of the molecule. The absorption maxima for **O-IDTBR** and **IDFBR** were at 690 and 530 nm, respectively (Fig. 12(a)). A strong and complementary absorption to **O-IDTBR** enabled the ternary blend films. Moreover, the difference in their physical properties resulted in a difference between **O-IDTBR** and **IDFBR** in the ternary blend: the less crystalline and more diffusive **IDFBR** dispersed in both P3HT and **O-IDTBR** phases (Fig. 12(b)), allowing the formation of a three-component redox cascade. As a result, the P3HT-based ternary blend showed an excellent photovoltaic performance with 7.7% PCE. Additionally, this

ternary device exhibited an outstanding dark and photostability in air. Fully solution-processed R2R compatible modules using **IDTBR**[95] (Note that **IDTBR** is the same compound as **O-IDTBR**. In this review, we use both abbreviated names based on the original papers.) and P3HT were performed by Machui et al.[48] A total module area of 60 cm^2 was fabricated and a PCE of 5.00% was achieved. The details are provided in Section 6.2.

A2–A1–D–A1–A2 modelled linear molecular structure was utilized to design and synthesize benzo[*d*][1,2,3]triazole (BTA)-containing NFA (**BTA1**), where rhodanine, BTA, and IDT were used as A2, A1, and D units, respectively.[97] **BTA1** had a flat backbone configuration, which was beneficial for the charge transport. The P3HT:**BTA1**-based device provided a high V_{oc} of 1.02 V and a high PCE of 5.24%. The utilization of thiazolidine-2,4-dione as the terminal unit keeping the central unit intact as **BTA1** developed a NFA (**BTA2**).[98] The substitution of sulphur atoms with oxygen atoms led to the increase of the LUMO energy level from -3.55 to -3.38 eV. The P3HT:**BTA2**-based device exhibited a doubled V_{oc} of 1.22 V compared to that of P3HT:$PC_{61}BM$ system, and a good PCE of 4.5%.

Two NFAs (**BT2** and **BT2b**) were also developed.[99] The high LUMO energy level of these two acceptors induced a high V_{oc} over 0.9 V when pairing with P3HT. The P3HT:**BT2b**-based device showed a high PCE of 6.08%, which was attributed to the red-shift absorption and the high crystallinity of the **BT2b** and the balanced electron and hole mobility of the blend films. 2-(1,1-Dicyanomethylene)rhodanine (RCN)-attached small molecule acceptor (**BTA3**) was developed using the A2–A1–D–A1–A2 modular strategy.[100] A lower weight ratio of 1:0.3 was applied for the P3HT:**BTA3** blend film. The P3HT:**BTA3**-based blend film exhibited a promising PCE of 5.64%. The higher electron mobility of the P3HT:**BTA3** film formed a continuous electron transport pathway. This study indicated that the incorporation of a weak electron-accepting building unit (BTA) is an effective design to improve the performance of RCN-attached NFAs. An incorporation of the methoxy groups into **BTA** provided **BTA101** and **BTA103**.[101] This methoxy groups contributed to upshifting the LUMO energy levels and facilitating the intramolecular charge transfer. **BTA101** gave one of the highest V_{oc} of 1.34V, and **BTA103** provided a PCE of 5.31%. In continuation with this material development using quinoxaline as a bridging unit gave new NFAs **Qx1b** and **Qx3b**, which gave PCEs of 4.81 and 6.37%, respectively.[102,103] In this BTA series, **BTA43** and **BTA53** were also developed by introducing the oxygen atoms into the side chains. Blending of **BTA43** and **BTA53** with P3HT provided high PCEs of 6.56 and 6.31%, respectively.[104] Introduction of the benzyl group on the terminal N atoms in the RCN part in **BTA3** gave a new NFA **BTA5**. This molecule showed a 6.01% of PCE.[105]

Chen et al. replaced the BTA unit with thiophene fused-BTA in **BTA3**-type molecule, which gave **JC2** and **JC14**. OSCs based on **JC2** and **JC14** showed PCEs of 6.24 and 7.72%, respectively [106, 107].

Two A–D–A type NFAs, **l-IDTBTRh** and **a-IDTBTRh**, comprising l-IDT or angular indaceno[2,1-*b*:6,5-*b*']dithiophene (a-IDT) as the central cores, BT as the π-bridge acceptor segments, and 3-ethylrhodanine as the end-capping groups, were synthesized.[108] The geometric shape of the l-IDT and a-IDT subunits had a pivotal role in governing the optoelectronic properties, charge mobilities, morphologies, and photovoltaic characteristics of the two acceptors. The P3HT:**l-IDTBTRh** based film offered a PCE of 5.38%.

Two thiazole (Tz) containing small molecular acceptors (**H-IDTzR** and **P-IDTzR**) with A–π–D–π–A type structures and different side chains were designed and synthesized.[109] Both compounds exhibited a good planar configuration due to incorporation of S•••N noncovalent conformational locks. **P-IDTzR** with bulky side chains exhibited suitable crystallinity, which adequately matches with P3HT. The P3HT:**P-IDTzR** blend films demonstrated optimal morphologies, thus achieved a higher PCE of 5.01% compared to the P3HT:**H-IDTzR** blend films (3.53%).

A NFA (**ORCN**) was designed by simple replacement of alkyl side chains in **ERCN** with alkoxy chains.[110] In **ORCN**, the HOMO and LUMO energy levels were increased by the alkoxy chains. Additionally, the S…O noncovalent conformational locks of alkoxy chains increased the planarity and rigidity of the backbone of acceptors, yielding higher crystallinity and better charge-transport mobility. Thus, the P3HT:**ORCN** blend films exhibited a higher PCE of 6.40%, compared to that of the P3HT:**ERCN** films (2.64%).

A π-extended NFA (**IDT-DPP-R**) containing the IDT unit was synthesized, exhibiting a strong near-infrared (NIR) absorption.[111] The P3HT:**IDT-DPP-R** binary blend provided a PCE of 1.42%. Ternary blend devices of two acceptors **IDT-DPP-R** (20%), $PC_{61}BM$ (80%), and P3HT exhibited a PCE of 3.95%.

Yu. et al. reported a simplified NFA named **A1** analogues to **O-IDTBR** for reducing the synthetic complexity.[112] This molecule showed a PCE of 5.39% after with an industrial readiness factor (i-FOM) of 0.26, which enhanced more than 30%, compared to the P3HT:**O-IDTBR** OSCs.

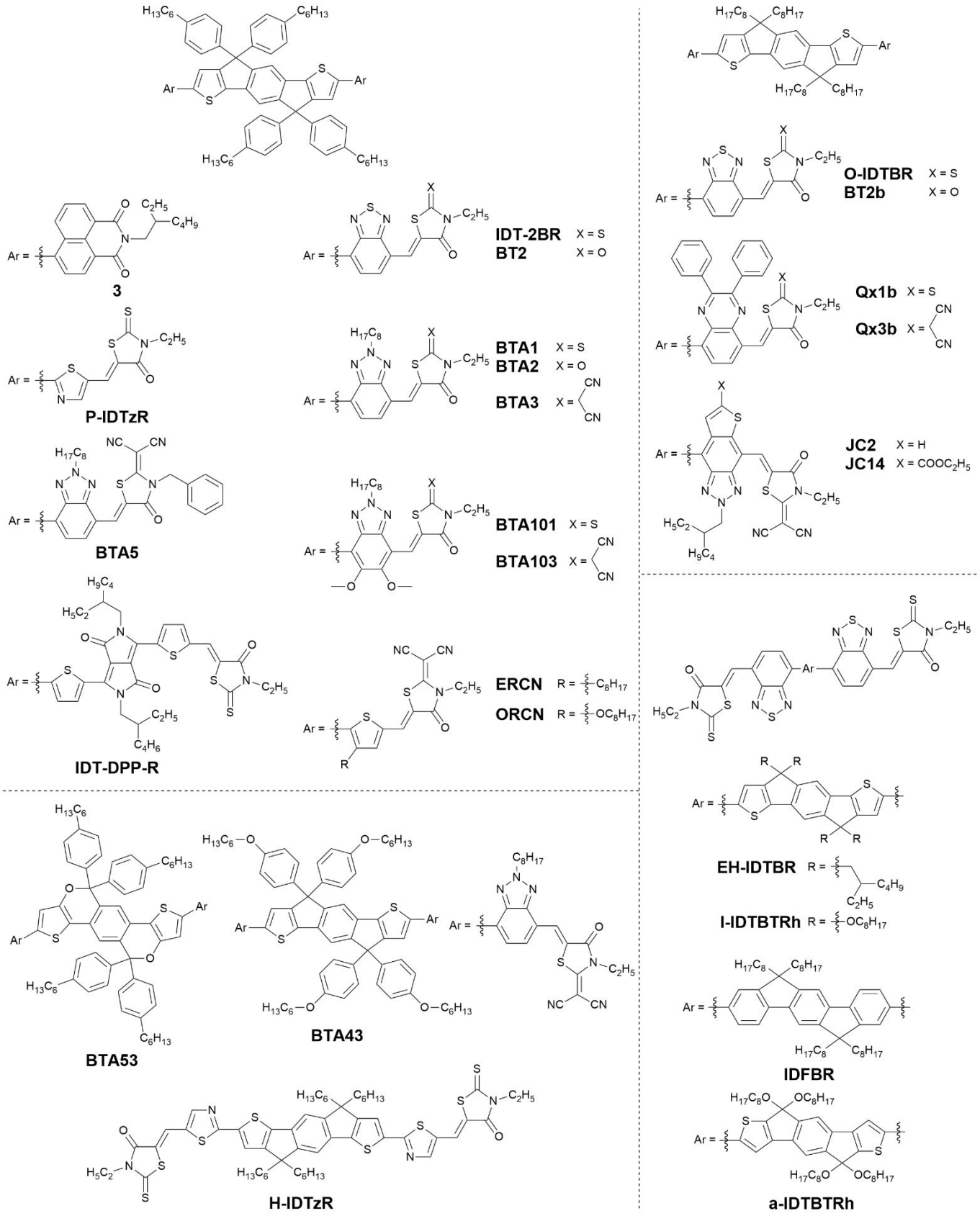

Fig. 11 Chemical structures of NFAs with a five-membered conjugated unit.

Table 4. Properties, photovoltaic characteristics, and blend film properties of NFAs with five-membered conjugated unit

Acceptor	LUMO /eV	HOMO /eV	E_g /eV	D:A ratio	Process solvent	V_{oc} /V	J_{sc} /mA cm^{-2}	FF	PCE /%	μ_e [a] /cm^2 V^{-1}s^{-1}	μ_h [a] /cm^2 V^{-1}s^{-1}	Ref
IDT-2BR	−3.69	−5.52	1.68	1:0.6	*o*-DCB[b]	0.84	8.91	0.68	**5.12**	2.6 x 10^{-4}	2.8 x 10^{-4}	93
3	−3.68	−5.67	2.25	1:1	*o*-DCB	1.06	4.85	0.46	**2.36**	4.22 x 10^{-4}	1.31 x 10^{-4}	94
O-IDTBR	−3.88	−5.51	1.63	1:1	CB	0.72	13.9	0.6	**6.34**	3-6 x 10^{-6}	3-7 x 10^{-4}	95
IDFBR	−3.70	−5.75	2.10	1:1	CB	0.89	7.4	0.68	**4.5**	NR	NR	96
BTA1	−3.55	−5.51	1.85	1: 0.6	*o*-DCB[c]	1.02	7.34	0.70	**5.24**	3.2 x 10^{-5}	1.8 x 10^{-6}	97
BTA2	−3.38	−3.55	2.00	0.6:1	CF[d]	1.22	6.15	0.60	**4.50**	3.4 x 10^{-4}	4.9 x 10^{-4}	98
BT2b	−3.56	−5.41	1.75	1:1	CF	0.92	10.02	0.66	**6.08**	8.4 x 10^{-5}	6.1 x 10^{-5}	99
BTA3	−3.61	−5.49	1.88	1:0.5		0.90	9.64	0.65	**5.64**	1.75 x 10^{-4}	1.60 x 10^{-6}	100
BTA103	−3.64	−5.37	1.77	0.5:1	CF	0.94	8.56	0.66	**5.31**	3.52 x 10^{-5}	1.46 x 10^{-6}	101
Qx3b	−3.63	−5.27	1.59	5:4	CF	0.75	12.87	0.66	**6.37**	2.0 x 10^{-5}	1.9 x 10^{-4}	103
BTA43	−3.47	−5.44	1.78	1:0.5	CF	0.89	10.84	0.68	**6.56**	3.2 x 10^{-6}	2.4 x 10^{-4}	104
JC2	−3.73	−5.48	1.75	1:0.8	CF	0.71	13.96	0.63	**6.24**	4.54 x 10^{-5}	5.02 x 10^{-5}	106
JC14	−3.63	−5.41	1.78	1:0.6	CF[e]	0.76	16.04	0.63	**7.72**	4.55 x 10^{-5}	7.49 x 10^{-5}	107
I-IDTBTRh	−3.68	−5.42	1.65	1:0.8		0.86	8.81	0.71	**5.38**	1.15 x 10^{-5}	2.32 x 10^{-6}	108
P-IDTzR	−3.44	−5.31	1.89	1:1	CF	1.02	9.00	0.55	**5.01**	7.08 x 10^{-6}	9.0 x 10^{-5}	109
ORCN	−3.56	−5.37	1.64	1:1.3	CF	0.87	11.5	0.62	**6.40**	1.83 x 10^{-4}	8.49 x 10^{-5}	110
IDT-DPP-R	−3.55	−5.39	1.44	1:1	CB[f]	0.65	4.07	0.55	**1.42**	NR	NR	111

a) Blend film. Blend films including b) 3% of 1-chloronaphthalene, c) 0.08% of 1-chloronaphthalene, d) 0.8% of DIO, e) 0.5% of DIO, f) 1.0% of DIO.

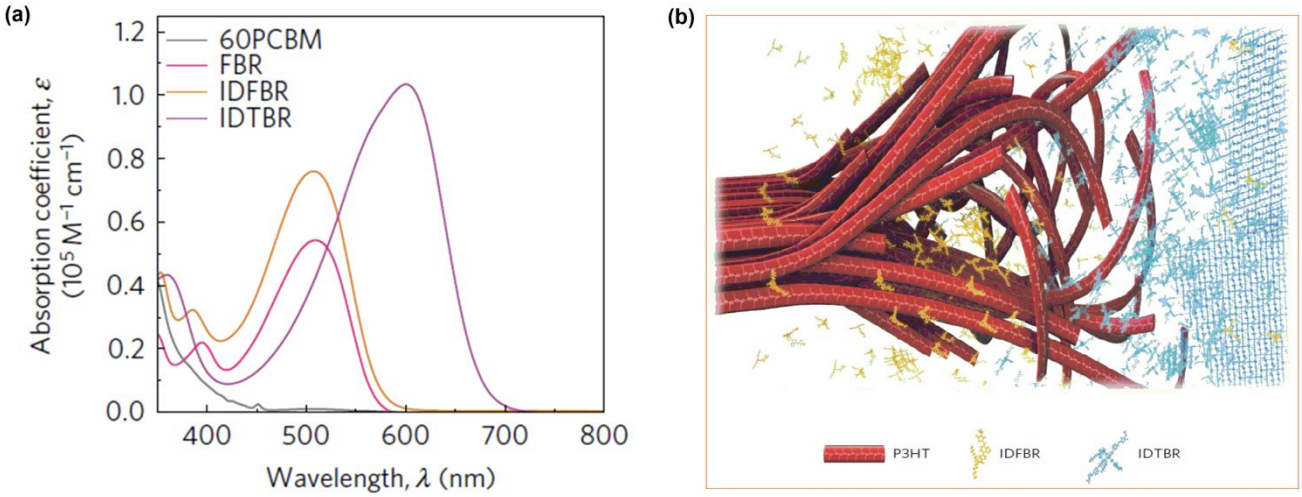

Fig. 12 (a) UV-vis absorption spectra of $PC_{61}BM$, FBR, **IDFBR**, and **IDTBR** in chloroform solutions. (b) Visual illustration of the binary P3HT:**IDTBR** blend with **IDFBR** presence, wherein the crystallinity of both P3HT and **IDTBR** is preserved. Reproduced with permission from ref 96. Copyright 2017, Nature Publishing Group.

3.6 NFAs with thiadiazole derivative in core:

π-Conjugated molecules bearing thiadiazole derivatives in the central unit have also been developed as NFAs (Fig. 13, Table 5). A high PCE of 2.54% with a high V_{oc} of 0.96 V was obtained by **PI-BT**, which is composed by a central benzotiadiazole unit and terminal imide units.[113] Crystallization behaviour of the molecules has influence on the PCEs.

It was proposed that the utilization of both the Channel-I and Channel-II processes (Fig. 2(c)) can achieve higher efficiencies beyond the Shockley-Queisser limit in OSCs.[114] Relying on this

hypothesis, a new NFA named as **YF25** was developed.[115] The P3HT:**YF25** film showed a PCE of 1.4%. It was confirmed that photo-induced hole transfer via acceptor excitation is a viable photocurrent generation pathway for maximising light harvesting in complementary acceptor-donor pairs. This is also supported by the time resolved microwave conductivity and external quantum efficiency (EQE) measurements.

Benzothiadiazole-based π-conjugated compoundS (**Imi-a-BT**) bearing phthalimide as electron-accepting terminal units were prepared.[116] The P3HT:**Imi-a-BT**-based OSCs showed a moderate photovoltaic performance with a PCE of 1.58%.The effect of alkyl chains on the phthalimide unit was further investigated by comparing five different alkyl chains.[117] The alkyl chains were found to have a strong influence on the energy levels and the crystallinity of the materials, and consequently the PCE of OSCs. A NFA named as **Ph-MH** with specific alkyl chain modification in the terminal part further improved the PCE up to 2.05%. The overall structural similarity of the NFAs facilitated to reveal the structure−property relationship; a good correlation between J_{SC} and the dispersion component of the surface energy (γ^d) of the NFAs was observed. (Fig. 14(a)) With the increased γ^d value, the molecular orientation gradually changed from the edge-on orientation to a more face-on orientation. This phenomenon is considered to be because the branched alkyl chain enhanced the amorphous behaviour and thus exposed more π-conjugated planes to the D:A interfaces, which has a beneficial effect for the efficient charge separation in the blend films (Fig. 14(b)).

Alkoxy-substituted benzothiadiazole (BT) was utilized to develop NFA (**BTDT2R**).[118] The P3HT:**BTDT2R**-based blend film exhibited a dramatic enhancement of PCE from 2.74% to 5.09% after solvent vapour annealing treatment.

PI and NI components are frequently used as terminal units for the construction of NFAs. Two electron-accepting π-conjugated molecules (**T-BTz-NI** and **T-BTz-PI**) were synthesized to investigate the influence of the terminal units on the properties and photovoltaic characteristics.[119] The utilization of NI led to red-shifted absorption and increased electron accepting characteristics, compared to those of PI. **T-BTz-NI** showed improved PCE of 1.16%.

Ie et al. utilized naphtho[1,2-*c*:5,6-*c*′]bis[1,2,5]thiadiazole (**NTz**) as an electron-accepting unit and synthesized a linear NFA (**NTz-Np**).[120] For the comparison, benzothiadiazole (BTz)-based NFA (**BTz-Np**) was also developed. Replacement of BTz with NTz facilitated the redshifted absorption and increased electron-accepting characteristics. The P3HT:**NTz-Np** blend film exhibited enhanced PCE as high as 2.81%, which is higher than that of the P3HT:**BTz-Np** based devices. This result showed the effectiveness of the NTz unit. A series of new NFAs bearing NTz as an electron-deficient central core coupled with a terminal Np via a thiophene linker containing various substituents (hydrogen, fluorine, hexyl, and 2-ethylhexyl groups) was developed to explore the effect of substituents on the thiophene linker on the properties and photovoltaic characteristics of the **NTz-Np** framework.[120] Among the examined substituents, **NTz-T$_{hex}$-Np** showed the highest PCE of 2.14% due to the good morphologies in the blend film.[121] Naphtho[1,2-*c*:7,8-*c*′]bis([1,2,5]thiadiazole (vNTz), which is a structural isomer of NTz, was also utilized as an electron-accepting unit in NFAs (**vNTz-T$_{eh}$R** and **vNTz-T$_{bo}$R**). The electrochemical and photophysical properties were nearly identical to the conventional material of **NTz-T$_{bo}$R** but the improved solubility allowed to utilize smaller alkyl chain. A PCE of 2.06% was obtained by **vNTz-T$_{eh}$R**. [122]

Ie et al. also established the synthesis of fluorinated naphtho[1,2-*c*:5,6-*c*′]bis-[1,2,5]thiadiazole (**FNTz**) as a new electron-accepting unit to be used in the NFA.[123] A FNTz-containing NFA (**FNTz-T$_{eh}$-FA**) was synthesized, in which thiophene linker and a fluoranthene imide (FA)-based terminal unit were utilized to increase the overall π-conjugation throughout the molecule. A high PCE of 3.12% was achieved when the P3HT:**FNTz-T$_{eh}$-FA** blend was used in OSCs.

Zhang et al. synthesized a new NFA named **ZY-4Cl** by replacing the cyanosubstituted end groups in **BTP-4Cl**[124] with the carbonyl-substituted counterpart.[125] To investigate the interaction between the donor and the acceptors, two model compounds (**TT-CN** and **TT-O**) were developed. This model study showed that the P3HT:**TT-CN** blend exhibited considerably stronger miscibility than that of the P3HT:**TT-O** blend. The difference in phase separation behaviours of these two blends was observed by atomic force microscopy (AFM) images; the 1:1 ratio of the P3HT:**TT-O** blend formed rough morphologies with roughness value (R_q) of 5.02 nm, whereas the P3HT:**TT-CN** blend showed smooth R_q of 1.53 nm (Fig. 15(a)). The P3HT:**BTP-4Cl**-based device showed a poor efficiency of 1.0% due to inferior phase separation. In contrast, the P3HT:**ZY-4Cl**-based device exhibited an inspiring new record PCE of 9.46%. From the GIWAX measurements, it was clear that there was no diffraction peaks in any directions for the P3HT:**BTP-4Cl** film, indicating the highly intermixed P3HT and **BTP-4Cl** phases and amorphous morphologies of the film. Moreover, the P3HT:**ZY-4Cl** film provided both edge-on and face-on orientations, reflecting that P3HT and **ZY-4Cl** have formed two separate phases in the blend film (Fig. 15(b)). Thus, it can be stated that lowering the miscibility via removing the cyano groups in the NFAs may be a feasible and universal method for improving the PCE of the P3HT:NFA-based OSCs. This is the best PCE to date for P3HT:NFA-based OSCs.

Quite recently, the P3HT:**ZY-4Cl** device exceeded a PCE of 10.24% by using a kind of volatilizable solid additive, SA4 (2-(thiophen-2-ylmethylene)-1*H*-indene-1,3(2*H*)-dione).[126] This enhancement was mainly due to the more ordered molecular packing and more favorable phase separation, leading to the enhanced charge transport and reduced carrier recombination. Thus, for the first time over 10% PCE was achieved using P3HT-based OSCs.

Zhou et al. reported **TPBT-RCN**,[127] which is analogous to the high performance NFAs Y5 and Y6. The P3HT:**TPBT-RCN**-based device exhibited an improved PCE of 5.11% in comparison with Y6 (PCE = 2.41%) and Y5 (PCE = 3.60%), owing to the suitable energy levels and optimized phase-separated morphologies.

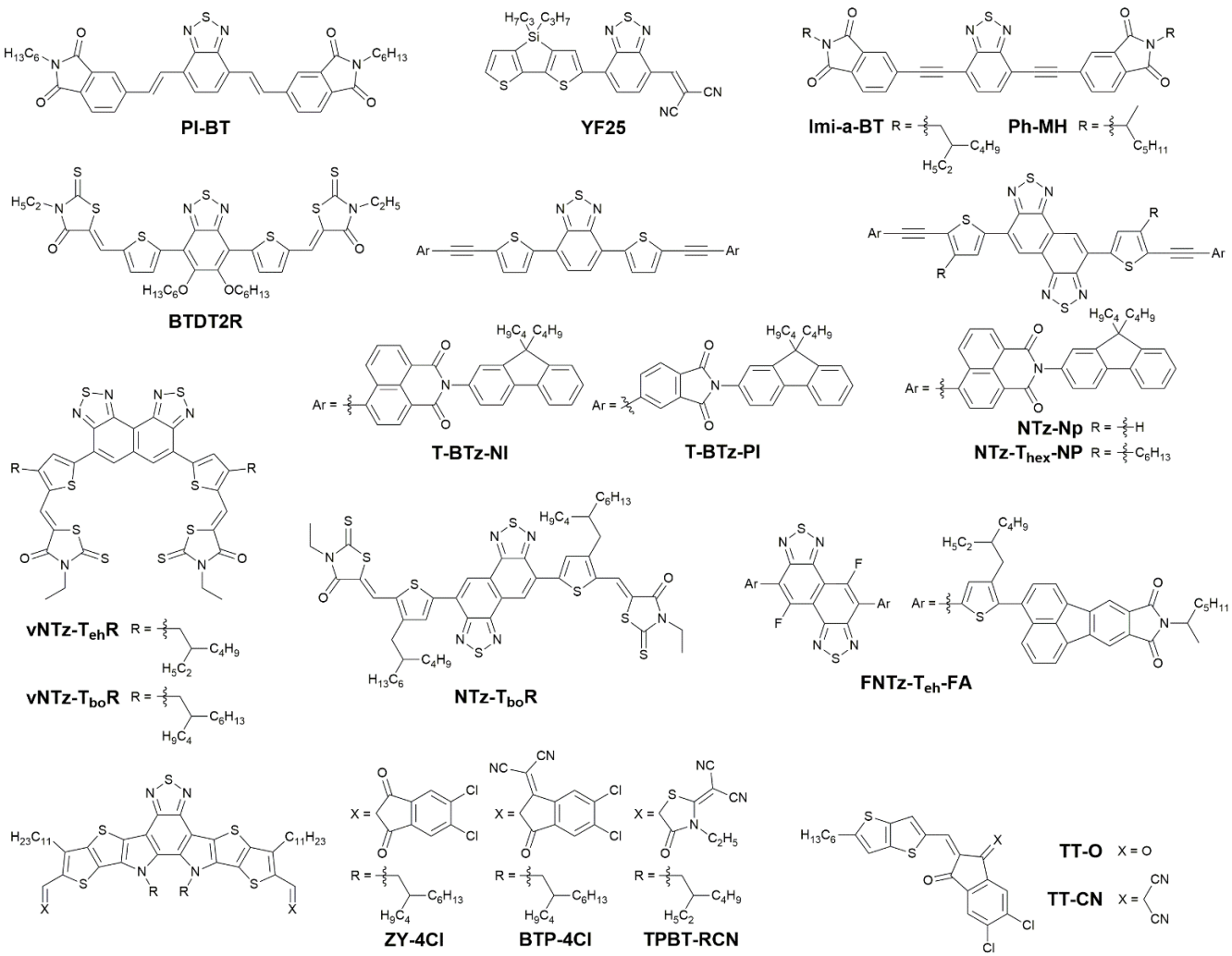

Fig. 13 Chemical structures of NFAs with thiadiazole central unit.

Table 5. Properties, photovoltaic characteristics, and blend film properties of NFAs with thiadiazole central unit

Acceptor	LUMO /eV	HOMO /eV	E_g /eV	D:A ratio	Process solvent	V_{oc} /V	J_{sc} /mA cm^{-2}	FF	PCE /%	μ_e [a] /cm^2 V^{-1}s^{-1}	μ_h [a] /cm^2 V^{-1}s^{-1}	Ref
PI-BT	−3.3	−5.8	2.34	1:2	CB	0.96	4.7	0.56	**2.54**	NR	NR	113
YF25	−3.7	−5.4	1.7	1:1.5	*o*-DCB	0.54	4.85	0.55	**1.43**	NR	NR	115
Imi-a-BT	−3.32	−6.21	2.58	NR	CB	0.89	3.99	0.45	**1.58**	5.4 x 10^{-6}	NR	116
Ph-MH	−3.31	−6.01	2.70	1:1	CF	0.76	5.59	0.48	**2.05**	3.3 x 10^{-6}	1.1 x 10^{-5}	117
BTDT2R	−3.73	−5.61	1.81	1:2	*o*-DCB	0.81	9.42	0.67	**5.09**	5.61 x 10^{-6}	1.68 x 10^{-4}	118
NTz-Np	−3.60	−6.01	1.73	1:1	CB:*o*-DCB (4:1)	0.90	5.18	0.60	**2.81**	1.6 x 10^{-5}	3.8 x 10^{-5}	120
vNTz-T$_{eh}$R	--	--	2.18	1:1	CF	0.68	6.34	0.48	**2.06**	NR	NR	122
FNTz-T$_{eh}$-FA	−3.55	−6.17	2.08	1:1	CB	0.89	5.81	0.60	**3.12**	2.8 x 10^{-6}	6.5 x 10^{-5}	123
ZY-4Cl	−3.67	−5.64	NR	1:1	THF	0.88	16.49	0.65	**9.46**	3.60 x 10^{-5}	7.08 x 10^{-5}	125
ZY-4Cl	--	--	--	1:1	No data [b]	0.90	17.00	0.67	**10.24**	--	--	126
TPBT-RCN	−3.71	−5.42	NR	1.1.5	THF	0.81	10.29	0.61	**5.11**	5.32 x 10^{-4}	5.52 x 10^{-4}	127

a) Blend film b) 15.6 wt % of SA4.

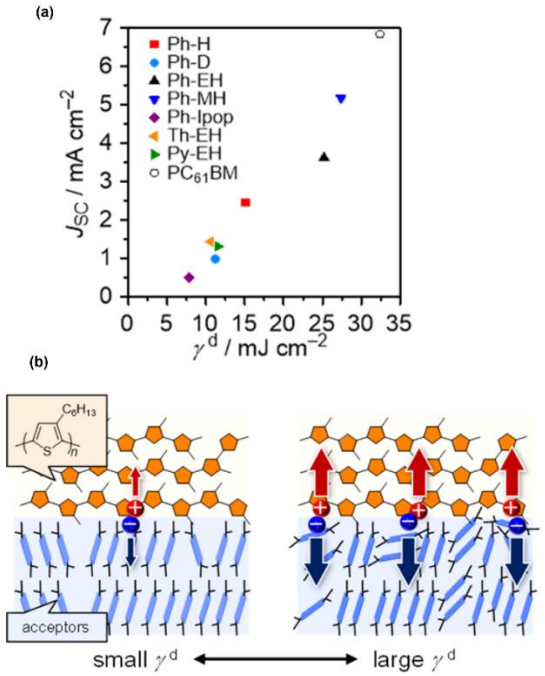

Fig. 14 (a) Plot of γ^d vs. *J*sc values for acceptor materials. (b) Graphical representation of the molecular orientation at donor-acceptor interfaces. Reproduced with permission from ref 117. Copyright 2016, American Chemical Society.

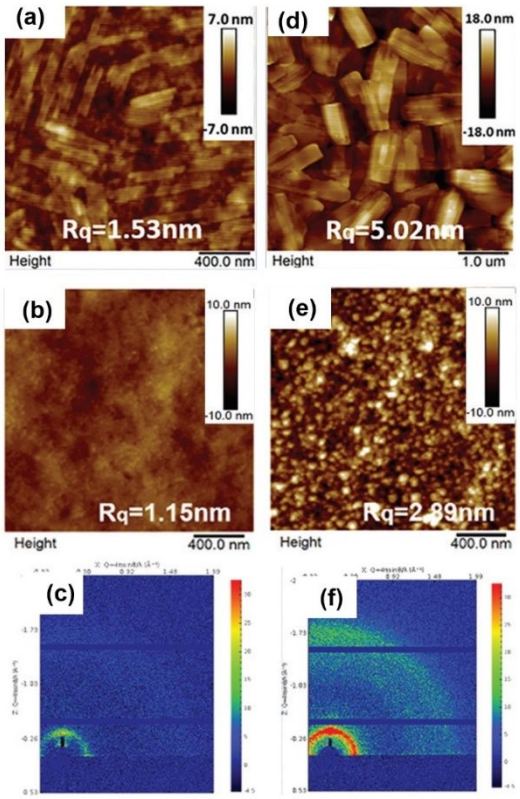

Fig. 15 (a) AFM images of P3HT:**TT-CN** and P3HT:**TT-O** blends at different weight ratios. (ii) AFM (a) height, (b) phase images, and (c) GIWAXS pattern of the P3HT:**BTP-4Cl** blend film. AFM (d) height, (e) phase images, and (f) GIWAXS pattern of the P3HT:**ZY-4Cl** blend film. Reproduced with permission from ref 125. Copyright 2020, Royal Society of Chemistry.

3.7 NFAs with DPP unit in core:

The DPP group can be introduced for the terminal unit, as summarized in Section 3.4, and also for the central unit in NFAs (Fig. 16 and Table 6). Sonar et al. developed DPP-based NFA named as **TFPDPP** to fabricate the P3HT:**TFPDPP** blend film, which achieved a PCE of 1.00%.[128]

An acetylene-bridged small molecule (**DPP-Pht$_2$**) based on DPP core end-capped with phthalimide was developed.[129] Suitable fibrillar microcrystalline domains in the P3HT:**DPP-Pht$_2$** film produced a better self-organization with the donor, resulting in a PCE of 3.28%.

A DPP-based small molecule (**DPP(C$_2$T)$_2$**) bearing ester groups at both α and β-positions in the end-capped thiophene ring showed ambipolar characteristics.[130] The combination of P3HT with **DPP(C$_2$T)$_2$** exhibited a PCE of 1.08%.

NFA named as **MPU1** was synthesized by the combination of the DPP core with terminal rhodanine.[131] The P3HT:**MPU1** blend film showed a PCE of 2.16%.

The influence of spacer unit between DPP and terminal imide unit was investigated.[132] The P3HT:**DPP-Th** and P3HT:**DPP-Tz** devices achieved PCEs of 1.30 and 0.43%, respectively, and this difference mainly originates from the film morphologies.

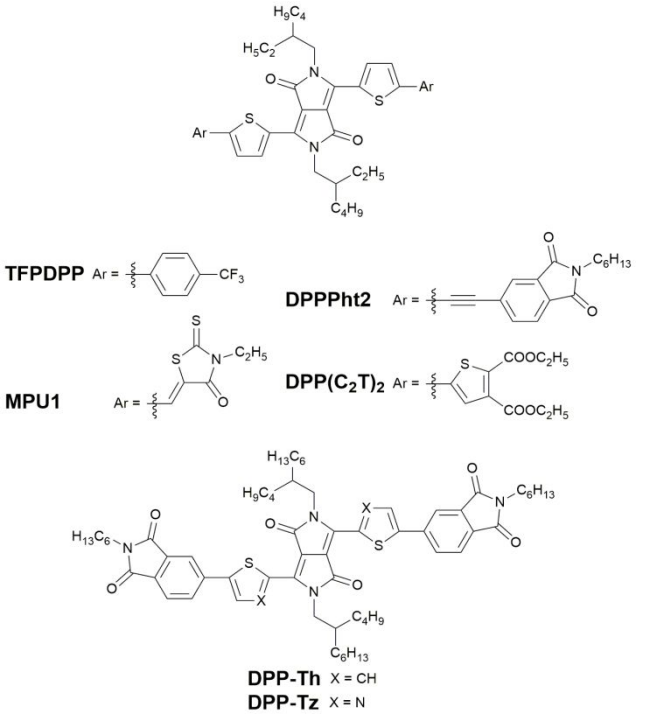

Fig. 16 Chemical structures of NFAs with DPP core.

3.8 3D type NFAs:

As summarized in Section 3.2, PDI-based NFAs bearing 3D structure have been developed. In this section, we summarize other 3D NFAs (Fig. 17, Table 6). Sauvé et al. developed unique 3D chemical structures based on azadipyrromethene (ADP) dyes and their zinc complexes named as **Zn(ADP)$_2$** and **Zn(WS3)$_2$** (Fig. 18(a)(b)).[133] These molecules showed intense absorption in the visible to NIR regions (Fig. 18(c)) and low

reduction potentials, leading to the suitable frontier energy level to combine with P3HT (Fig. 18(d)). The most-efficient NFA **Zn(WS3)$_2$** prevented crystallization and promoted favourable nanoscale phase separation from P3HT blend (Figs. 18(e)–(h)), providing a high PCE of 4.10%.

The effect of a fluorine atom in three different positions on the **Zn(WS3)$_2$**[133] was further explored by synthesizing four different compounds **Zn(L*n*)2** (where *n*=1–4).[134] Fluorine substitution had a slight effect on the absorbance and energy levels. However, it strongly affected charge transport, bimolecular recombination, and device performance. The fluorine substitution increased the PCEs from 2.5% (**Zn(WS3)$_2$**) to 3.7% (**Zn(L3)$_2$**). The introduction of hexyl groups at the para position of the proximal phenyls in **Zn(WS3)** produced **Zn(L1)$_2$**.[135] **Zn(L2)$_2$** is derived from **Zn(L1)$_2$** with 1-naphthylethynyl groups at the pyrrolic positions. A PCE of 5.5% was obtained for the P3HT:**Zn(L2)$_2$** based blend film.[136]

The DPP-based 3D molecule (**4**) having a [2,2]paracyclophane framework in the central unit yielded the highest PCE of 2.69%.[137]

A spirobifluorene (SF) unit was utilized to generate a 3D NFA **SF-DPPEH**.[138] The unique X-shaped molecular structure originating from the spiro linkage resulted in high solubility and suppressed aggregation. Moderate crystallization behaviour and nanoscale phase separation decreased geminate recombination and thus enhanced the PCE up to 3.63%. SF-functioned 3D NFAs (**SF-OR** and **SF-ORCN**) using rhodanine or 2-(1,1-dicyanomethylene)rhodanine as the terminal units were developed.[139] **SF-OR** and **SF-ORCN** showed high PCEs of 6.66 and 4.48%, respectively. The incorporation of cyano group into rhodanine core improved the electron accepting ability. However, it sacrificed the ordered structure because the conjugated backbone became less planar.

Chen et al. introduced a SF-based 3D NFA (**SF(DPPB)$_4$**), which had a symmetrical cruciate configuration.[140] This structure assured fine phase separation in the active layer. The P3HT:**SF(DPPB)$_4$** films exhibited a PCE of 5.16% and a high V_{oc} of 1.14 V. This PCE was further improved to 6.09% by using an inverted device structure.[141] **SF(DPPFB)$_4$** was synthesized using SF core and four DPP arms with end-capping by 4-fluorobenzene.[142] The terminal fluorine atoms decreased the energy levels of **SF(DPPFB)$_4$**. In particular, its LUMO energy level decreased by 0.04 eV, compared to that of **SF(DPPB)$_4$**.[140] The P3HT:**SF(DPPFB)$_4$**-based device exhibited a PCE of 4.42%. The spiro(fluorene-9,9'-xanthene) unit was functionalized with terminal DPP units to generate 3-D NFA named as **SFX1**.[143] With the P3HT combination, a PCE of 6.55% was achieved after post-annealing treatment.

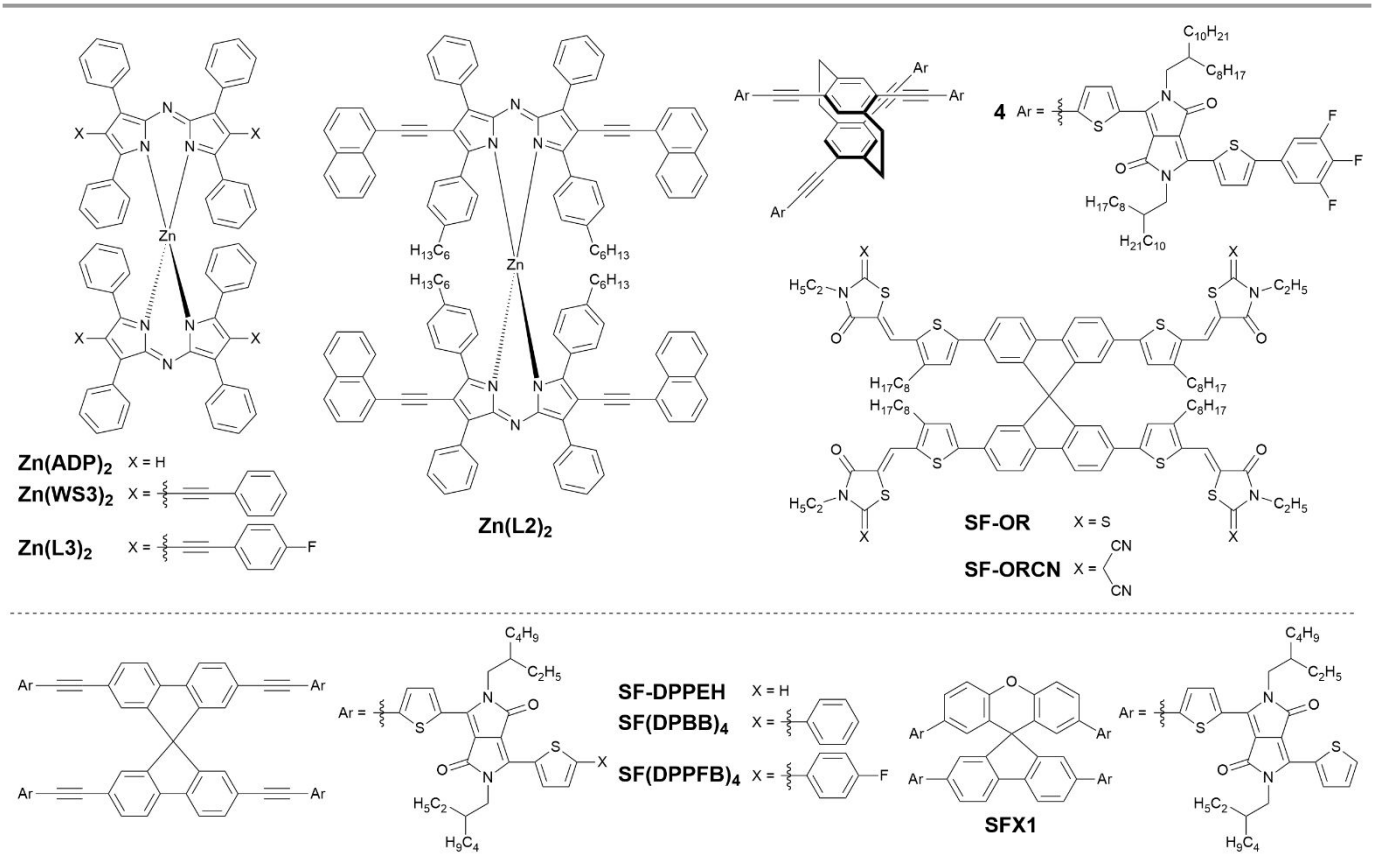

Fig. 17 Chemical structures of 3D NFAs.

Table 6. Properties, photovoltaic characteristics, and blend film properties of NFAs with DPP central unit and 3D NFAs

Acceptor	LUMO /eV	HOMO /eV	E_g /eV	D:A ratio	Process solvent	V_{oc} /V	J_{sc} /mA cm^{-2}	FF	PCE /%	μ_e [a] /cm^2 V^{-1}s^{-1}	μ_h [a] /cm^2 V^{-1}s^{-1}	Ref
TFPDPP	−3.52	−5.26	1.94	1:2	Toluene	0.81	2.36	0.52	**1.00**	2.17 x 10^{-3}	2.17 x 10^{-3}	128
DPP-Pht$_2$	−4.13	−5.88	1.65	1:2	CF	0.89	5.91	0.50	**3.28**	1.5 x 10^{-4}	NR	129
DPP(C$_2$T)$_2$	−3.78	−5.37	1.52	1:2	CF	0.92	3.63	0.33	**1.08**	2.78 x 10^{-6}	1.22 x 10^{-5}	130
MPU1	−3.99	−5.81	1.82	1:1	CF[b]	0.60	6.54	0.55	**2.16**	8.15 x 10^{-5}	2.58 x 10^{-5}	131
DPP-Th	−4.1	−5.8	1.7	1:2	CF	0.86	3.25	0.37	**1.30**	1.00 x 10^{-6}		132
Zn(WS3)$_2$	−3.85	−5.60	1.75	1:0.7	*o*-DCB	0.77	9.1	0.59	**4.10**	1.9 x 10^{-4}	2.1 x 10^{-4}	133
Zn(L3)$_2$	−3.87	−5.66	1.59	1:0.7	*o*-DCB	0.73	8.5	0.60	**3.7**	2.6 x 10^{-3}	5.5 x 10^{-4}	134
Zn(L2)$_2$	−3.84	−5.54	1.54	1:1.5		0.82	11.3	0.59	**5.5**	2.4 x 10^{-5}	3.1 x 10^{-4}	135
4	−3.53	−5.29	1.76	2:1	NR	0.90	5.88	0.51	**2.69**	2.05 x 10^{-5}	5.87 x 10^{-4}	137
SF-DPPEH	−3.60	−5.26	1.66	1:1	CF	1.10	6.96	0.48	**3.63**	NR	NR	138
SF-OR	−3.25	−5.50	2.25	1:1	CF	0.97	7.30	0.63	**4.66**	6.71 x 10^{-6}	8.49 x 10^{-5}	139
SF(DPPB)$_4$	−3.51	−5.26	1.75	2:1	CF	1.14	8.29	0.55	**5.16**	1.5 x 10^{-4}	8.65 x 10^{-5}	141
SFX1	−3.82	−5.67	1.85	1:1.2	*o*-DCB	0.95	11.20	0.61	**6.54**	2.20 x 10^{-4}	NR	143

a) Blend film. b) Including 3% of DIO.

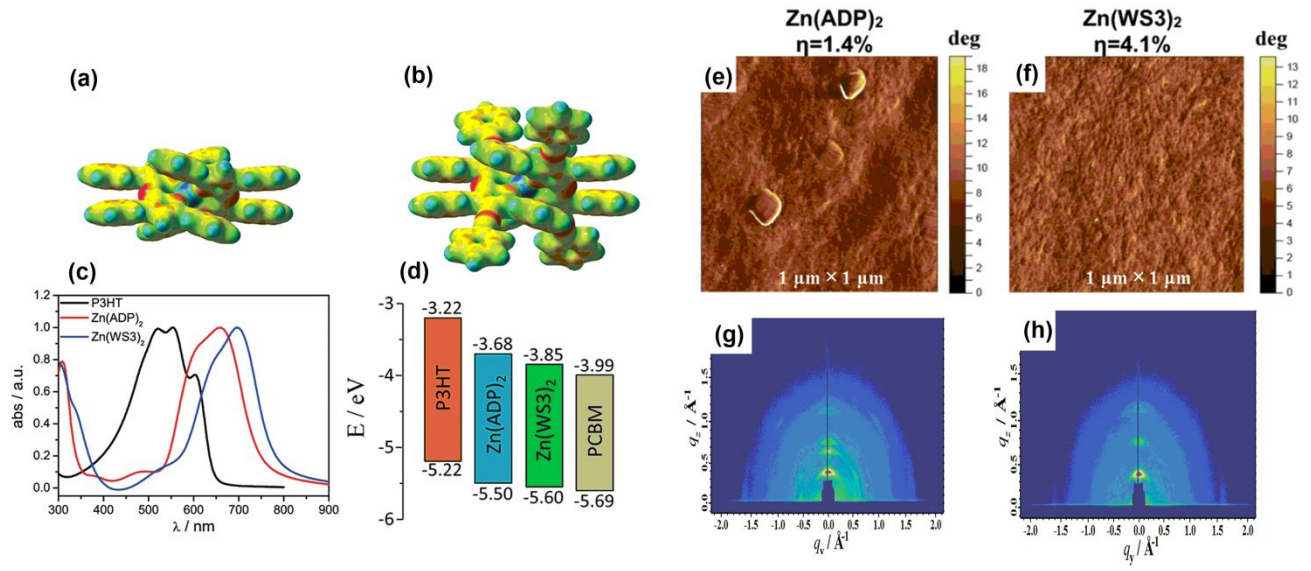

Fig. 18 3D NFAs of (a) **Zn(ADP)$_2$** and (b) **Zn(WS3)$_2$** (c) Energy level diagrams of donor and acceptors. (d) UV–vis absorption spectra of P3HT, **Zn(ADP)$_2$** and **Zn(WS3)$_2$** in films. (e) AFM phase images of annealed active layers of P3HT:**Zn(ADP)$_2$** and (f) P3HT:**Zn(WS3)$_2$** (g) GIWAXS data of annealed P3HT:**Zn(ADP)$_2$** and (h) annealed P3HT:**Zn(WS3)$_2$** films. Reproduced with permission from ref 133. Copyright 2014, John Wiley & Son.

3.9 Star-shaped NFAs:

Relatively planar and two-dimensional (2D) NFAs have also been developed (Fig. 19, Table 7). Lin et al. introduced a star-shaped NFA named as **S(TPA–DPP)** based on triphenylamine (TPA) as a core and DPP as arms. The HOMO and LUMO energies were -5.26 and -3.26 eV, respectively, and the difference between the LUMO of **S(TPA–DPP)** and the HOMO of P3HT was as large as 1.5 eV, resulting in a high V_{oc} of 1.18V with a PCE of 1.20%.[144]

An isoindigo-based star-shaped acceptor (**P1**) with triphenylamine and phenyl cores was explored. OSCs based on the P3HT:**P1** blend film exhibited a PCE of 0.81%.[145]

Tetraphenylethylene (TPE) core-based NFA (**4D**) with DPP terminals was synthesized.[146] **4D** had a four-directional

molecular arrangement with excellent solubility. This compound showed a PCE of 3.86% with a high V_{oc} of 1.18 V. The TPE unit was terminally flanked with cyanopyridone (CP) unit to generate a 3D molecular architecture to provide an NFA named as **TPE-CP4**.[147] When **TPE-CP4** was combined with P3HT, it produced a high PCE of 6.02%. Recently another NFA named **W8**, which possesses NDI as terminal units, was reported to achieve a PCE of 5.26%.[148]

A promising NFA, TrBTIC, composed of electron rich truxene (Tr) core and electron-deficient dicyano indanedione with BT moiety was developed.[149] TrBTIC exhibited excellent solubility in common solvents including 1,2,4-trimethylbenzene (TMB), a green solvent, but crystallized slowly with long-term aging in TMB at room temperature. The P3HT:TrBTIC-based blend film showed an improved PCE from 6.62% to 8.25% due to the pre-phase separation of the donor and acceptor, in the blending condition. This detail is shown in Section 5.

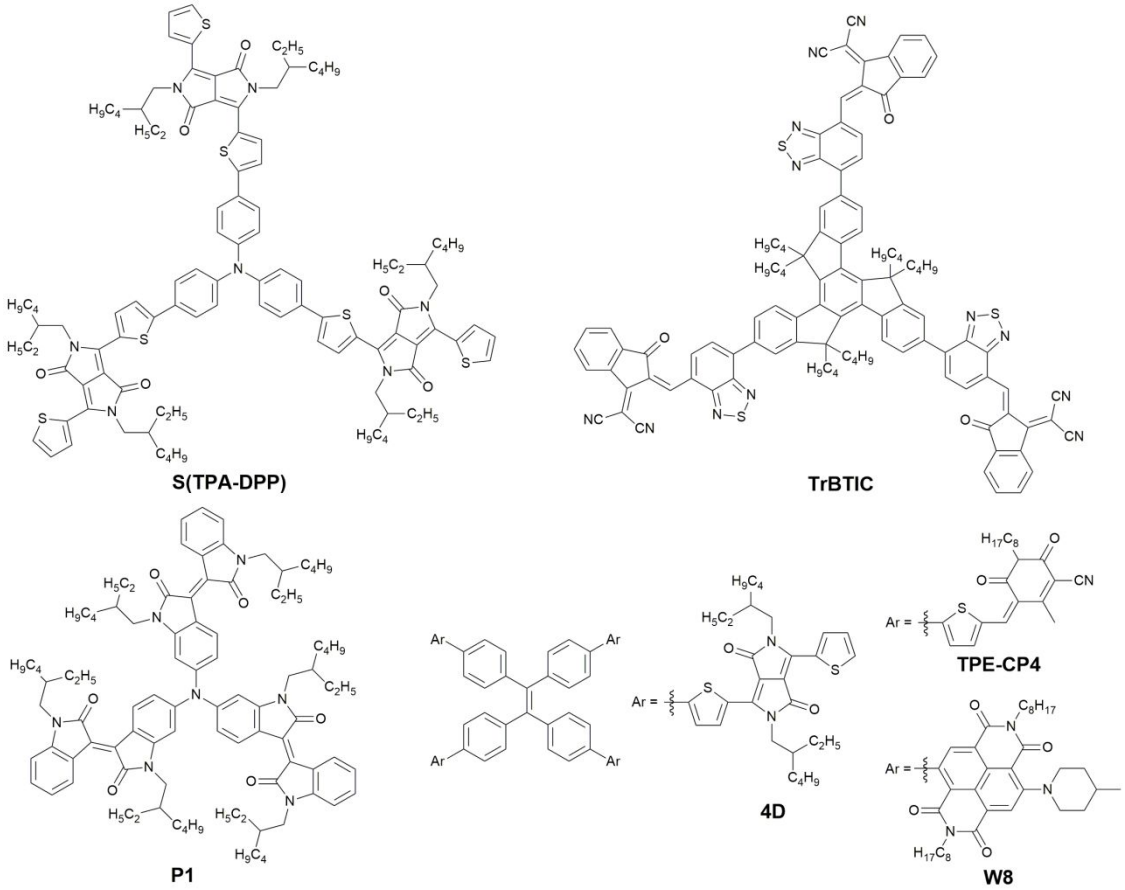

Fig. 19 Chemical structures of NFAs

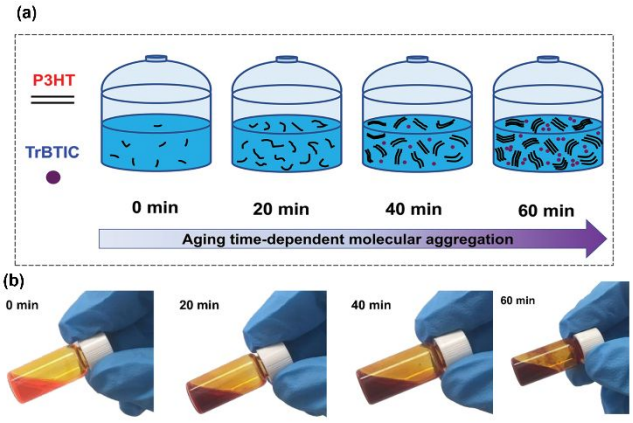

Fig. 20 (a) Schematic illustration of the P3HT: **TrBTIC** aggregation stage in TMB solution (b) Photographs of pristine P3HT solution (8 mg/mL in TMB) after different aging times. Reproduced with the permission from ref 149. Copyright 2019 John Wiley & Sons.

3.10 Miscellaneous NFAs:

Novel NFAs that do not fit the categories in previous sections are summarized here (Fig. 20, Table 7). A new type of NFAs using strain and Hückel aromaticity was reported by Wudl et al.[143] In this study, 9,9'-bifluorenylidene backbone was designed to develop a series of electron-accepting compounds. An asymmetric **D99'BF** showed higher solubility and suitable energy levels (HOMO = -5.17 eV and LUMO = -3.24 eV). The P3HT:**D99'BF**-based OSCs showed a PCE of 1.7% with a promising high V_{oc} of 1.10 V. It was revealed that electron transfer can occurs with very low LUMO energy offset (~0.12 eV) between P3HT and **D99'BF**.[150, 151]

Electron-accepting pentacene-based π-conjugated molecules were developed by Anthony et al.[152] It was noticed that the photocurrent was strongly correlated with the crystal

packing motif of pentacene derivatives; 2D π-stacking interactions showed lower photovoltaic characteristics than one-dimensional π-stacking interactions. Compound **5** showed the best performance with a PCE of 1.27%. The dicyanoethylene-substituted quinacridone derivative (**DCN-*n*CQA**, *n* = 4, 6, and 8) was developed.[153] The **DCN-8CQA** exhibited a low LUMO energy level (-4.1 eV), small bandgap (1.8 eV), and moderate electron mobility. The P3HT:**DCN-8CQA**-based OSCs showed a PCE of 1.57%.

Park et al. developed a dicyanodistyrylbenzene-based NFA (**NIDCS**), in which a specific strategy for modulating the self-assembly tendencies was implemented by combining a NI moiety into the terminal positions of the molecules.[154] The bulkiness of the NI substituent weakened the intermolecular interactions, and balanced aggregation characteristics were obtained in the blend film. The **NIDCS**-based OSCs with P3HT exhibited a PCE of 2.71% an exceptional high J_{sc} of 8.04 mA cm^{-2}.

An all-carbon NFA material (**DIR-2EH**) based on diindeno[1,2-*g*:1′,2′-*s*]rubicene was developed.[155] This is a molecular fragment of fullerene, and thus has high electron affinity. A high content of acceptor in the blend film with P3HT (D:A ratio of 1:4) yielded the best PCE of 3.05%. Solution-processable 1,6,7,10-tetramethylfluoranthene (**6**), as the smallest fragment of fullerene, was synthesized for NFA application.[156] This molecule showed absorption up to 400 nm, yielding a PCE of 0.71%. However, this device showed high stability under air-exposed conditions.

A NFA having fused thieno[3,2-*b*]thiophene (TT) named as **DNIT-TT2T** was synthesized.[157] The P3HT:**DNIT-TT2T**-based blend film achieved a PCE of 1.25%.

Two NFAs named **DRCN3TT** and **DRCN5TT** with A–D–A type chemical structures based on thieno[3,2-*b*]thiophene central unit and 2-(1,1-dicyanomethylene)rhodanine terminal group were developed. These compounds showed both donor and acceptor characteristics. The appropriate LUMO energy levels of -3.50 eV for **DRCN3TT** and -3.52 eV for **DRCN5TT** allowed to act as appropriate electron acceptors for the P3HT donor.[158] The **DRCN3TT** and **DRCN5TT**-based blended films with P3HT exhibited PCEs of 3.55 and 2.78%, respectively.

Thickness-tolerable BHJ OSCs were fabricated using **IDTIDT-IC** as an NFA with D–A type donor polymer.[159] Using **IDTIDT-IC**, the P3HT-based OSCs showed an impressive PCE of 3.64% at a large active layer thickness of 236 nm.[160] This thickness-insensitive photovoltaic characteristic of the P3HT:**IDTIDT-IC** system enabled large-scale R2R processing. This is described in Section 6.2.

Silicon phthalocyanines (SiPcs) based NFA, bis(tri-n-butylsilyl oxide) SiPc (**(3BS)$_2$-SiPc**)[161] was developed and a high PCE of 3.6% was achieved with the SiPcs-based material, for the first time.

Recently, utilising the indacenodithieno[3,2-b]thiophene (IDTT) as central part and rhodanine as a terminal part and joined them with a ring-locked by carbon-carbon double bond to get a NFA, **IDTT-CR**. The P3HT: **IDTT-CR** blend produced a PCE of 2.86%.[162]

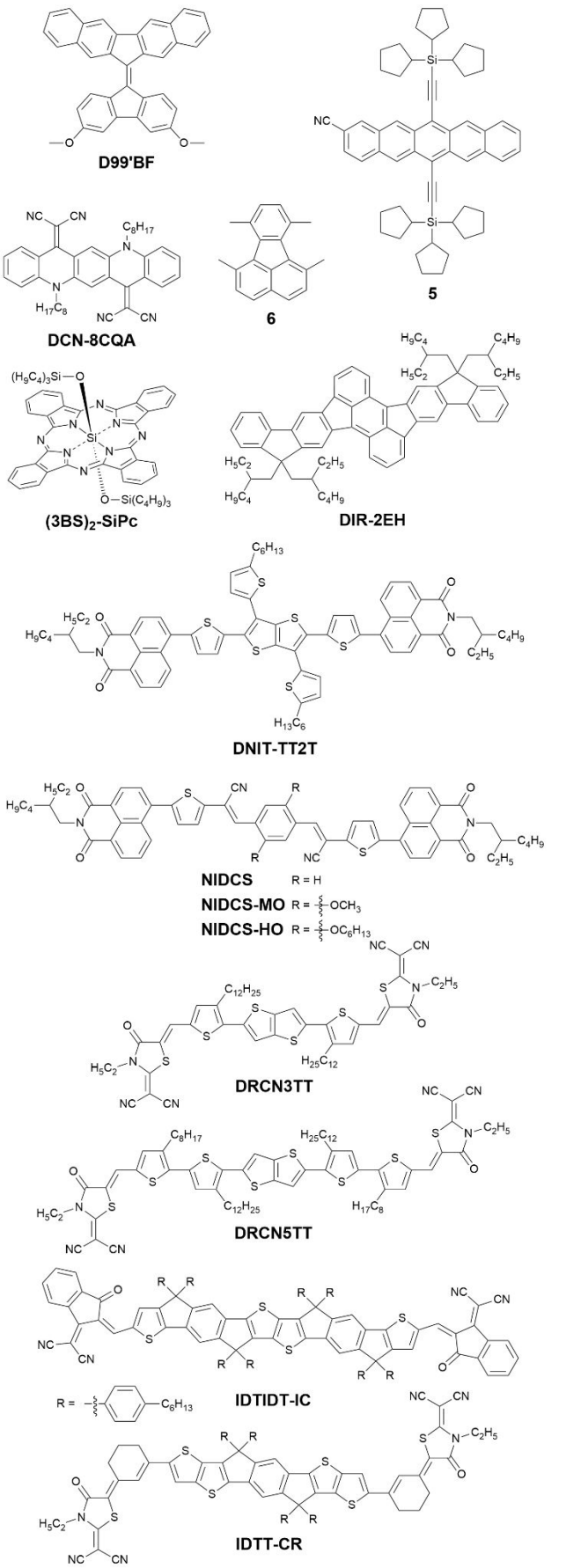

Fig. 21 Chemical structures of miscellaneous NFAs.

Table 7. Properties, photovoltaic characteristics, and blend film properties of star-shaped and miscellaneous NFAs

Acceptor	LUMO /eV	HOMO /eV	E_g /eV	D:A ratio	Process solvent	V_{oc} /V	J_{sc} /mA cm^{-2}	FF	PCE /%	μ_e [a] /cm^2 V^{-1}s^{-1}	μ_h [a] /cm^2 V^{-1}s^{-1}	Ref
S(TPA–DPP)	−3.26	−5.26	1.85	1: 1	*o*-DCB	1.18	2.68	0.38	**1.20**	6.8 x 10^{-6}	2.8 x 10^{-4}	144
P1	−3.77	−5.54	1.77	1:1	*o*-DCB	0.96	1.91	0.44	**0.81**	NR	NR	145
4D	−3.81	−5.53	1.72	1:1.2	*o*-DCB	1.18	5.17	0.64	**3.86**	NR	NR	146
TPE-CP4	−3.90	−5.72	1.82	1:1.2	*o*-DCB	0.99	9.68	0.63	**6.02**	10^{-3}	NR	147
TrBTIC	−3.62	−5.56	1.80	1:1.2	TMB	0.88	13.04	0.72	**8.25**	3.3 x 10^{-4}	3.6 x 10^{-4}	149
D99'BF	−3.37	−5.58	2.22		*o*-DCB	1.10	3.90	0.40	**1.70**	NR	NR	150
DCN-8CQA	−4.1	−5.90	1.80	1:1	CF/DCB	0.48	5.72	0.57	**1.57**	1.14 x 10^{-4}	NR	151
NIDCS	−3.42	−5.90	2.48	1:2.5	CF	0.73	8.04	0.46	**2.71**	5.65 x 10^{-8}	2.0 x 10^{-5}	152
DIR-2EH	−3.30	−5.38	2.08	1:4	*o*-DCB	1.22	4.29	0.58	**3.05**	1.26 x 10^{-8}	NR	153
DNIT-TT2T	−3.75	−5.94	2.19	1:1	CB	0.88	3.38	0.44	**1.25**	NR	NR	157
DRCN3TT	−3.50	−5.44	1.72		CF	0.90	7.87	0.50	**3.55**	1.48 x 10^{-4}	8.18 x 10^{-5}	158

a) Blend film.

4. Acceptor polymers in P3HT-based OSCs:

All-polymer solar cells (all-PSCs) are a class of OSCs in which the active layers are composed of an p-type polymer (donor) and an n-type polymer (acceptor).[163] In the polymer:polymer blend films, critical issues such as inadequate light-harvesting capability, low charge-carrier mobility, and formation of unfavourable film morphologies have become more prominent.[164,165] A number of effective strategies has been developed to control film properties and morphologies for all-PSCs, and PCE values over 10% have recently been possible by the combination of D–A type donor and acceptor polymers.[166-168] For recent advances in all-PSCs, please go through some reviews.[169-173] In the case of P3HT-based all-PSCs, acceptor polymers should have well-matched absorbance, crystallinity, and morphologies with P3HT. However, appropriate acceptor polymers to be used with P3HT are limited, and thus the PCEs are still positioned around 5%. In this section, we focus on acceptor polymers for P3HT-based all-PSCs.

4.1. Acceptor polymers based on fluorene and benzothiadiazole units:

The pioneering work of P3HT-based all-PSC was accomplished by the utilization of **F8TBT** as an acceptor polymer (Fig. 22, Table 8).[174] This was achieved by the incorporation of an electron-accepting BT unit into polymer backbone. The lowered energy levels allowed efficient electron transfer from P3HT to **F8TBT**. Later, nanopatterned P3HT:**F8TBT** films fabricated by a nanoimprinting technique improved the PCE to 1.9%.[175] The optimization of interconnected phase-separated domains was reported using crystalline P3HT nanowire blended with **F8TBT**, which showed a PCE of 1.87%.[176] The **F8TBT** acceptor polymer with substituents in the BT unit was also reported. The alkoxy-substituted **F8TBT-OC6** showed a PCE of 1.80% with a V_{oc} of 1.36.[177] In 2011, a PCE of 2.0% was attained by using **F12TBT**.[178] The PCE of the P3HT:**F12TBT** solar cells was further increased to 2.7% through the use of **F12TBT** with a high M_w of 78,000 g mol^{-1}.[179] The high M_w **F12TBT** could form suitable blend morphologies for efficient charge generation and charge transport after thermal annealing. The nanoscale characterization of the electrical properties of the P3HT:**F12TBT** films using the conductive AFM was effective to optimize the blend morphologies, and the chloroform-processed P3HT:**F12TBT** films reached a PCE of 3.5%.[180]

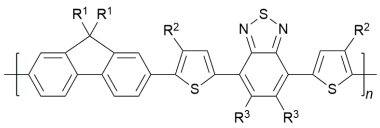

F8TBT R^1 = C_8H_{17} R^2 = C_6H_{13} R^3 = H
PF12TBT R^1 = $C_{12}H_{25}$ R^2 = H R^3 = H
PFDTBT-OC6 R^1 = C_8H_{17} R^2 = H R^3 = OC_6H_{13}

Fig. 22 Chemical structures of acceptor polymers based on fluorene and BT units.

4.2. NDI-based acceptor polymers:

Among myriads of rylene dimide families, NDI and PDI were extensively utilized as electron-accepting units to construct

acceptor polymers with high μ_e.[181,182] Facchetti et al. developed an NDI-based renowned polymer (**P(NDI2OD-T2)**), which exhibited high μ_e values of 10^{-3} cm^2 V^{-1} s^{-1} in space-charge-limited current (SCLC) measurements and 0.85 cm^2 V^{-1} s^{-1} in OFETs.[181,183] Researchers were keen to apply **P(NDI2OD-T2)** to an acceptor polymer in all-PSCs.

In 2011, Sirringhaus et al. and Loi et al. independently reported all-PSCs based on P3HT:**P(NDI2OD-T2)**,[184,185] where only modest PCEs of 0.16–0.18% were achieved. The formation of large domains (~100 nm) in the blend, driven by preferential segregation and crystallization,[186] and rapid geminate recombination of the charge population (within 200 ps of excitation), was the governing factor behind the relatively poor J_{SC}, which limited the overall device performance.[184] However, a high FF approaching 65% could be achieved, demonstrating that once excitons are formed, the charges can be effectively transported for collection at the respective electrodes. Later, the morphologies of the P3HT:**P(NDI2OD-T2)** films were optimized by the process solvent: changing the process solvent from xylene to xylene: chloronaphthalene (1:1) mixed solvent enhanced PCEs up to 1.3%, which is primarily attributed to the enhanced J_{SC} as the result of suppressed self-aggregation of **P(NDI2OD-T2)** (Fig. 23, Table 8).[187,188]

In 2012, Jenekhe et al. reported crystalline acceptor polymers of NDI copolymerized with bisselenophene named as **PNDIBS**. All-PSCs comprised of **PNDIBS** and P3HT showed a PCE of 0.9%.[189] The EQE spectrum of this device showed that approximately 19% of the photocurrent came from the NIR (700–900 nm) light harvesting by **PNDIBS**. D–A type block copolymers (**P3HT-PNBI-P3HT**), which consist of regioregular P3HT and NDI units, have been reported.[190] The All-PSCs fabricated using the P3HT:**P3HT-PNBI-P3HT** blend film achieved a reasonable PCE of 1.28%. A series of NDI-based copolymers with varying number of fused thiophenes as donor units was developed. Among them, **P(NDI-4fTh)** showed the highest μ_es in OFETs and PCEs in OSCs.[191]

The low-lying (~4.0 eV) LUMO energy level of **P(NDI2OD-T2)** is one of the main reasons of low V_{oc} for all-PSCs (~0.4 V) when combined with P3HT. Considering this, Tajima et al. synthesized a new alternating copolymer named as **PF-NDI**, which was comprised of NDI and fluorene (F), a common electron-donating building block.[192] As the twisting structure between NDI and F units led to the localization of LUMO density in the NDI unit, **PF-NDI** had a high-lying LUMO energy level (-3.61 eV). All-PSCs using **PF-NDI** showed a PCE of 1.63% with enhanced V_{oc} of 0.68V.

A series of three-component acceptor polymers (**P[$PDI_{x\%}$-co-$NDI_{(1\_x)\%}$]**) having indaceno[2,1-b:6,5-b']dithiophene (IDT), NDI, and PDI units was synthesized, and the highest all-PSC performance of 1.54% PCE was found when x = 25.[193] The comparison of device performance using a binary blend of P3HT:**$PPDI_{25}$-co-NDI_{75}** with a ternary blend of P3HT:**PPDI100**:**PNDI100** employing the same PDI, NDI, and IDT component molar ratio showed that the ternary blend showed inferior performance, due to the ambiguous phase separation.

Angular-shaped NDI was designed to increase the LUMO level of polymers.[194] Although the acceptor polymers having this unit showed a low PCE of 0.32%, one of the highest V_{oc} up to 0.94 V was achieved for all-PSCs.

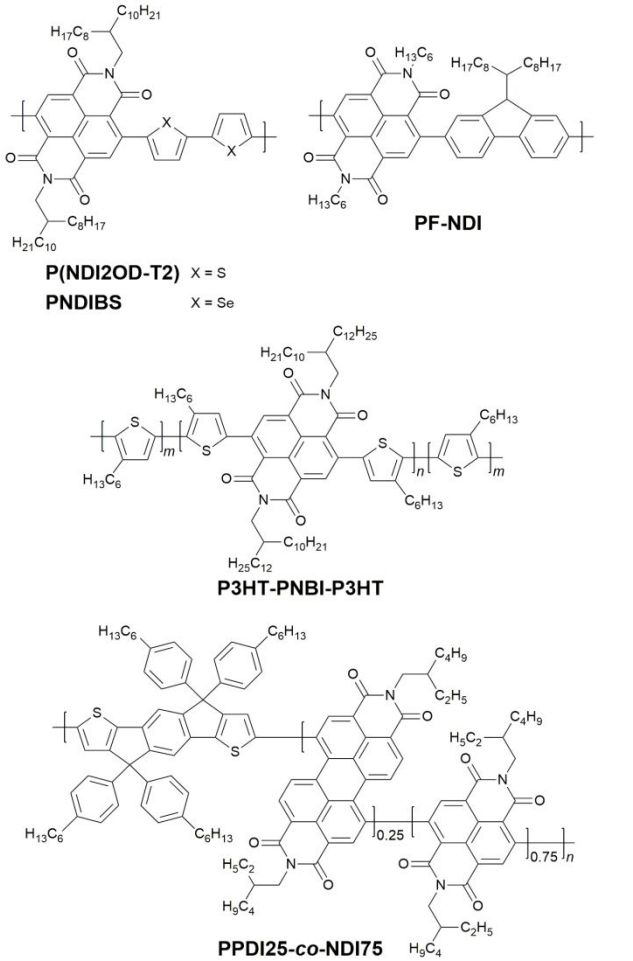

Fig. 23 Chemical structures of NDI-based acceptor polymers.

4.3. PDI-based acceptor polymers:

PDI-based copolymers generally have low-lying LUMO levels of approximately ~3.9 eV, and an absorption edge of approximately 650 nm. Thus, the D–A type donors with narrow bandgaps and deep HOMO energy levels are suitable partners to harvest more photons and achieve high V_{oc} over 1.0 V. In contrast, some of PDI-based copolymers have been also employed to construct the all-PSCs using P3HT as a donor.

Regio-regular copolymer (**r-PDI-diTh**) and regio-irregular copolymer (**i-PDI-diTh**) based on bithiophene and PDI units were developed (Fig. 24, Table 8).[195] This copolymer **r-PDI-diTh** showed superior performance to **i-PDI-diTh**. Utilizing **r-PDI-diTh** with P3HT as donor and employing the inverted device configuration, a PCE of 2.17% was achieved by the appropriate vertical phase separation. The chain-growth polymerization method was applied to the synthesis of copolymers based on bithiophene and PDI units, and these copolymers showed compatible PCEs compared to those synthesized by conventional methods.[196]

A–A type copolymers (**P1-Cn** and **P2-Cn**) composed by PDI and BT units were reported.[197] Due to the presence of ethynyl spacer between PDI and BT unit, **P2-Cn** showed red-shifted absorption and high electron mobility. However, all-PSCs based on polymeric acceptors and P3HT showed that the performance of **P1-Cn** device surpassed that based on **P2-Cn**, due to the high-lying LUMO energy level, efficient charge-separation, and good film morphologies.

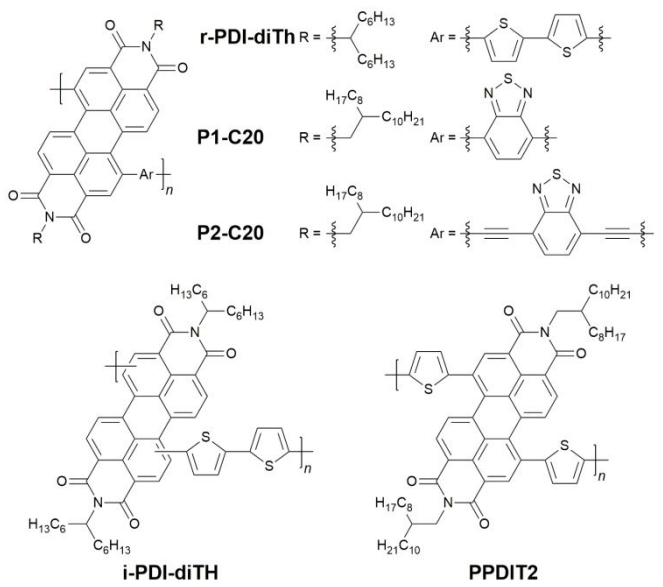

Fig. 24 Chemical structures of PDI-based acceptor polymers.

4.4. Other acceptor polymers:

The low absorption coefficient and fixed low-lying LUMO energy levels of NDI/PDI-based acceptor polymers are the major limitations for the PCEs of P3HT-based all-PSCs. Thus, new electron-accepting building units have been designed and applied to develop the acceptor polymers for all-PSCs.

New imide-annelated electron-accepting (TPTI) and dicyanomethlene-annelated units (CN) were synthesized and used to develop acceptor polymers with different monomer combinations.[198] All-PSCs comprised of **PNPDI** and P3HT showed a PCE of 0.75%. Copolymers having thiazole-flanked diketopyrrolopyrrole unit (DPP2TzT) showed broad absorbance up to NIR region.[199] All-PSCs based on P3HT and DPP2TzT-containing acceptors showed PCEs ranging from 1.5% to 3.0% and the solar cells exhibit a broad spectral response from 350 nm to 950 nm. An acceptor polymer (**P-BNBP-CDT**) composed of an alternating double B-N bridged bipyridine (BNBP) and a cyclopenta-[2,1-*b*:3,4-*b*']-dithiophene (CDT) units exhibited strong absorption in the visible range of 500–650 nm and suitable LUMO/HOMO energy levels for P3HT.[200] **P-BNBP-CDT** showed a PCE of 1.76% (Fig. 25, Table 8).

Ie et al. utilized fluorinated naphthobisthiadiazole (FNTz) to synthesize **FNTz-T-BTz**.[201] P3HT:**FNTz-T-BTz** based all-PSC showed reasonable photovoltaic characteristics of up to 1.13% PCE with a high V_{oc} of 0.96V. This efficiency was due to the good charge transporting characteristics and suitable blend film morphologies in the blend films.

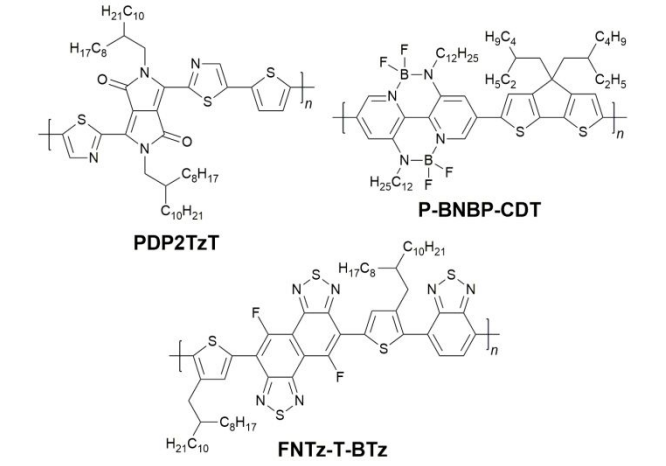

Fig. 25 Chemical structures of other acceptor polymers.

Table 8. Properties, photovoltaic characteristics, and blend film properties of acceptor polymers

Acceptor	LUMO /eV	HOMO /eV	E_g /eV	D:A ratio	Process solvent	V_{oc} /V	J_{sc} /mA cm^{-2}	FF	PCE /%	μ_e [a] /cm^2 V^{-1}s^{-1}	μ_h [a] /cm^2 V^{-1}s^{-1}	Ref
F8TBT	−3.15	−5.37	NR	1: 1	xylene	1.25	4.00	0.45	**1.8**	8.0 x 10^{-5}	8.0 x 10^{-4}	174
PFDTBT-OC6	-3.22	-5.30	NR	1:2	CF	1.36	2.93	0.45	**1.8**	NR	NR	177
F12TBT	-3.50	-5.50	NR	1:1	CF	1.19	2.93	0.42	**2.0**	NR	NR	179
P(NDI2OD-T2)	-4.00	-5.4	NR	1:1	Xyl:CN (1:1)	0.53	4.18	0.59	**1.31**	2.2 x 10^{-4}	3.4 x 10^{-4}	188
PNDIBS	−3.94	−5.93	NR	1:3	CF[b]	0.53	3.79	0.44	**0.9**	0.07	NR	190
PF-NDI	−3.61	−5.93	2.1	2:1	CB[c]	0.68	3.63	0.66	**1.63**	NR	NR	192
PPDI$_{25}$-co-NDI$_{75}$	−3.77	−5.65	1.88	3:1	*o*-DCB	0.68	3.62	0.62	**1.54**	3.0 x 10^{-5}	3.7 x 10^{-4}	193
r-PDI-diTh	−3.80	−5.50	1.68	1:1.5	*o*-DCB	0.52	7.65	0.55	**2.17**	5.0 x 10^{-4}	NR	195
P-BNBP-CDT	−3.45	−5.64	NR	5:1	CF	1.01	4.98	0.35	**1.76**	3.0 x 10^{-5}	2.31 x 10^{-4}	200
FNTz-T-BTz	−3.40	−5.71	1.74	1:1	*o*-DCB	0.96	2.63	0.46	**1.13**	9.8 x 10^{-5}	9.5 x 10^{-5}	201

a) Blend film. b) Including 1% of DIO. c) Including 0.5% of DIO.

5. P3HT:NFAs-based OSCs processed by nonhalogenated solvent:

Halogen-free organic solvents are sensible alternative as process solvents against conventional halogenated toxic solvents. The active layers of OSCs are mostly processed by halogenated toxic solvents such as CB, *o*-DCB, and CF in a cell size in laboratory. However, these solvents cannot be used for the fabrication of a module size OSC toward mass production due to environmental issues. Thus, fabrication of OSCs by halogenated toxic solvents is one of the crucial limiting factors for the commercialization of OSC. In this context, the development of P3HT:NFAs-based OSCs processed by nonhalogenated green solvents is urgently needed. However, studies on this topic are still in course, and the basic design principle of the NFAs that is compatible with the nonhalogenated green solvent process to obtain a reasonable performance of the OSCs is still a severe challenge. For the advances in D–A type donors:NFAs-based OSCs processed by various nonhalogenated green solvents, please go through some important reviews.[202,203] In this review, we focus on the research progress in the field of green-solvent-processed P3HT:NFA-based OSCs.

Anthony and Malliaras et al. utilized toluene as a nonhalogenated solvent to produce the P3HT:**2,3-CN2-TCPS-Pn (1c)** blend film.[204] This film formed large micro-size crystals, and the corresponding OSC showed a PCE of 0.43%. The utilization of toluene halogenated *o*-DCB mixed solvent improved film morphology by suppressing the crystallization of pentacene during film formation, resulting in the increase of PCE to 1.29%.[152]

Sonar et al. utilized toluene as a process solvent to fabricate the P3HT:**TFPDPP** blend film, which showed a PCE of 1.00%.[127] In contrast, the use of CF resulted in low PCE of 0.25%.

Brabec et al. utilized **IDTBR** to develop R2R production of OSC modules in various solvents.[48] Among the examined solvents, xylene and *o*-methyl anisole were effective, achieving high PCEs of 3.71 and 5.41%, respectively. Using methyl naphthalene as an additive to the xylene solution further improved the PCE from 3.71 to 4.99%.

Peng et al. developed a novel NFA named as **TrBTIC**.[149] They found that P3HT can be readily dissolved in 1,2,4-trimethylbenzene (TMB) in warm conditions and slowly crystallized at room temperature. By using this phenomenon, pre-phase separation between P3HT and **TrBTIC** occurred before the deposition of the solutions, which was tuned by adjusting the aging time. In fact, in this study, it was found that 40 min of aging time was the most appropriate phase separation time for this blend, producing uniform nanowires and favourable interpenetrating networks for exciton dissociation and charge transport, which resulted in a high PCE of 8.25% (Fig. 26).

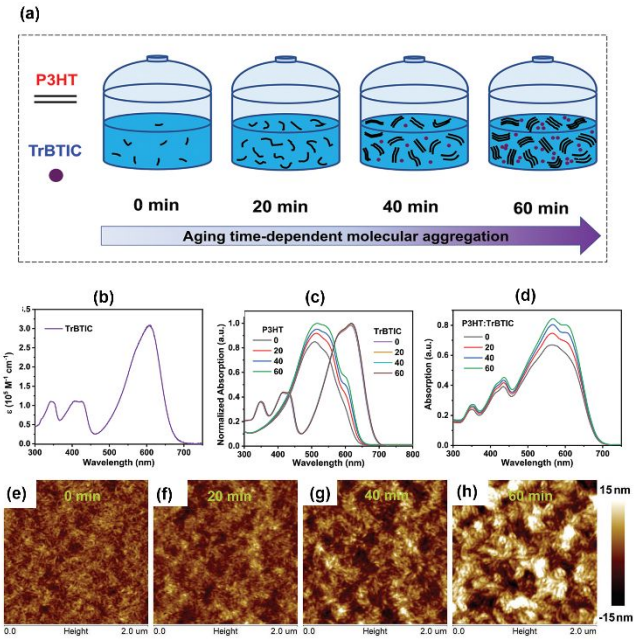

Fig. 26(a) Chemical structures of P3HT and **TrBTIC**. (b) Schematic illustration of the P3HT:**TrBTIC** aggregation stage in TMB solution. (c) Absorption coefficient profile of **TrBTIC** in TMB. (d) Aging time-dependent UV-vis absorption of P3HT and **TrBTIC** films. (e) Aging time-dependent UV-vis absorption of P3HT:**TrBTIC** (f) Photographs of pristine P3HT solution (8 mg/mL in TMB) after different aging times. Reproduced with permission from ref 149. Copyright 2019 John Wiley & Sons.

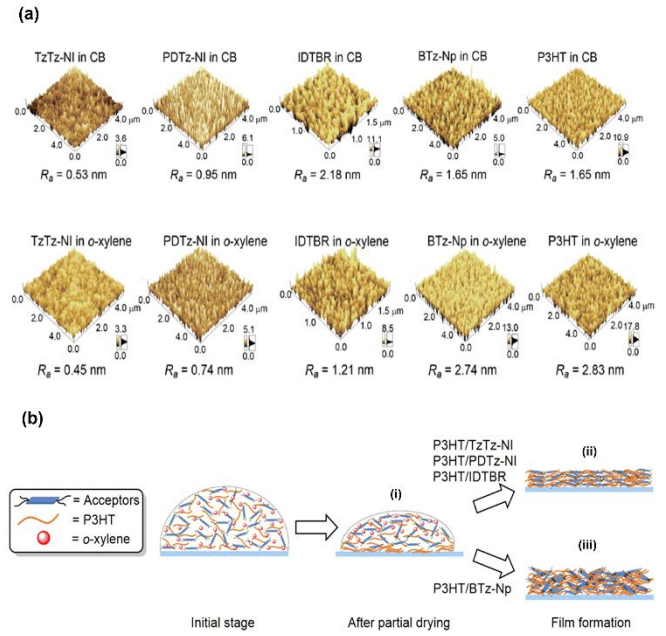

Fig. 27 (a) AFM height images of the pristine films for the acceptors and P3HT films processed using CB (top) and o-xylene (bottom). (b) Schematic representation of the possible phase separation processes during spin-coating for P3HT and acceptors in *o*-xylene solutions. Reproduced with the permission from ref 205. Copyright 2020 American Chemical Society.

As the polarity of the solvent has a substantial influence on controlling the miscibility of P3HT and NFA, the blend film morphology should be dictated by both the solvent polarity as well as the polar character of P3HT and NFA. Thus, the dipole moment of the compounds can be a decisive factor for controlling the overall morphology of the blend film depending on the solvent polarity. Considering this, Ie *et al.* focused on the correlation between the dipole moment of NFAs and the process solvents, because most nonhalogenated green solvents have low dipole moment.[205] Two NFAs named as **TzTz-NI** and **PDTz-NI** were developed. The symmetric fused central units of thiazolothiazole (TzTz), pyradinodithiazole (PDTz) contributed to decreasing dipole moment of the molecules. These acceptors showed improved PCEs when CB was replaced with *o*-xylene. The representative NFA of **IDTBR** showed the same tendency. In contrast, **BTz-Np** bearing a high dipole moment showed a decreased PCE. The *o*-xylene-processed P3HT:**TzTz-NI** and P3HT:**PDTz-NI** blend films showed smooth film morphologies and higher miscibility than the CB-processed films, which was attributed to the better film-forming characteristics.

Very recently, Zhang et al. synthesized a new NFA named **ZY-4Cl**.[124] THF-processed P3HT:**ZY-4Cl** based cell exhibited a record high PCE of 9.46%.

6. Large area fabrication of P3HT:NFA-based OSCs:

In this Section, we introduce a brief overview on the process technology of OSCs for large area fabrication, and then we discuss the upscaling procedure from cell size to module size for the efficient P3HT:NFA-based OSCs.

6.1. Requirement for large-scale OSC fabrication:

The large-area printing process of OSCs is the frontrunner in organic electronics research and development. Thus, it is regarded as one of the beginning footsteps towards the commercialization of OSCs. Donor and acceptor, which are solution-processable, low cost, and insensitive to the fabrication method, should be employed to fabricate the actual large area OSCs. However, the number of materials that fulfilled these points is still limited. Generally, spin-coating is a popular technique to prepare active layers of OSCs in the laboratory. Despite being the most approving choice, this method is not entirely applicable for large volume production since it leads to several unintentional and bewildering variations in fabricating device processing, affecting the overall PCE of the device. In addition, the loss of more than 90% of materials during spin-coating is also a problem. Therefore, for relatively long and flexible substrates, large-area R2R methodologies are accomplished for efficient device fabrication (Fig. 28).[206]

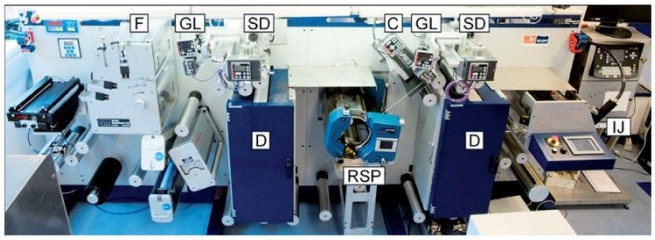

Fig. 28 R2R printing and coating machine for organic solar cells with: namely guideline detection (GL), strobe camera (C), and barcode inkjet printer (IJ) mounted on the R2R machine setup with flexo-printing (F), slot-die coating (SD), rotary-screen printing (RSP), and driers (D). Reproduced with permission 206 Copyright 2013, Wiley-VCH.

6.2. Towards the P3HT:NFAs-based OSCs: from Lab to fab

Because of the low PCE of the P3HT-based OSCs (usually below 4%), only D–A type polymer:fullerene-based OSCs were explored for the production in module size.[207] In this area, a comprehensive research on the large-scale production of OSCs from lab to the industry has been well documented by Krebs et al.,[208] who discussed about the complete manufacturing process in detail. Later, they have established the utility of OSC technology by demonstrating complete R2R production of a low bandgap copolymer, poly(dithienothiophene-*co*-dialkoxybenzothiadiazole) (PDTTDABT) with $PC_{60}BM$ in air, using slot-die coating, employing flexible substrates in their research. Solar cell modules embracing 16 serially connected cells were prepared with a total module active area of 96 cm^2. (Fig. 29).[209]

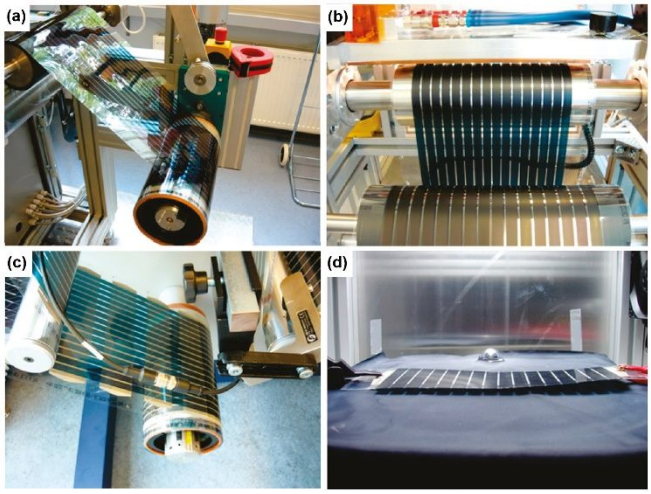

Fig. 29 (a) Pictures of R2R production with PDTTDABT. (a) Coating of active layer. (b) Coating of PEDOT layer. (c) Lamination of the finished modules and (d) test of single module under a solar simulator. Reproduced with permission from ref 209. Copyright 2010 American Chemical Society.

IDTBR is the newest NFA perfectly complimentary, with low cost P3HT-based donor, launched by S. Holliday and McCulloch et al.[90] Utilizing **IDTBR** with P3HT, a practical research of fully solution-processed R2R compatible modules was further performed by Machui et al. for the first time.[101] Nonhalogenated green solvents were also utilized to realize R2R process, which is fully compatible with industrial requirements. As **IDTBR** had a reasonably good solubility in various solvents, the blending condition of the active layer was optimized with respect to the solubility of P3HT. The solubility requirement of P3HT was fixed at more than 10 mg/mL at 90 °C for all the solvents. Thus, the P3HT-solvent solubility distance as a function of the boiling point of the solvent was established (Fig. 30). Finally, it was revealed that solvents located closer to the green box in Fig. 29 provide better performances.

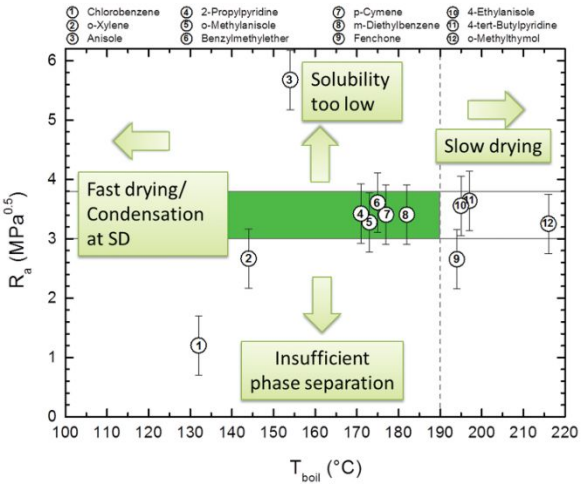

Fig. 30 P3HT-solvent solubility distance as a function of the boiling point of the solvent. The upper horizontal grey line (1), lower grey line, (2) and vertical dashed line (3) represent boundary conditions. Solvents in the green box are defined as 'suitable for processing' SD: slot-die. Reproduced with permission from ref 48. Copyright 2018 Royal Society of Chemistry.

Furthermore, these OSCs were successfully produced in module size. These OSCs are composed of 12 individual cells monolithically connected in series with an active total area of 64 cm^2 (8 x 8 cm). One individual cell, including interconnect, has a length of 0.67 cm (8 cm/12 cells) and an area of 5.33 cm^2 (64 cm^2/12 cells) (Fig. 31). A total module area of 60 cm^2 could be fabricated, and a PCE of 5.0% was achieved with halogenated solvent, which was almost retained when the active layers of the modules were processed from nonhalogenated green solvent (4.7%).

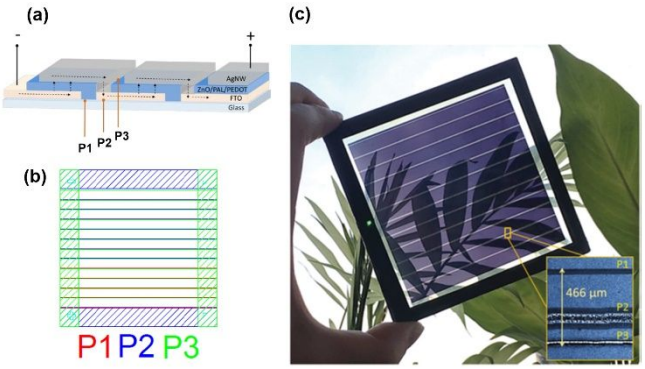

Fig. 31 (a) Schematic diagram of the module device architecture with the patterning lines P1, P2, and P3. (b) Module layout with the structuring lines P1, P2 and P3. (c) Image of a semi-transparent module based on P3HT:IDTBR processed from CB:BrA, with a confocal microscope image of the interconnect region. Reproduced with permission from ref 48. Copyright 2018 Royal Society of Chemistry.

Thus, this is the first time that the P3HT:NFA-based OSCs was produced in module size with almost 5.00% stable PCE, which provides new perspectives in this research field.

Conclusions and outlook

In this review, we summarized the development of NFAs compatible with low cost and wide bandgap donor polymer P3HT. Some important classes of electron-accepting materials have emerged to accelerate the advancement in this field. After the progressive rise of narrow band gap D–A type donor polymer, the P3HT-based OSC researches became insufficient. However, it is still a relevant research field as many high performance NFAs with unique molecular design are continuously emerging. As recent researches are approaching the commercial barrier of almost 9.0–10.0% PCE[125,126,149] for P3HT:NFA-based OSCs, the commercialization of the OSCs is close. The key points toward the further development of P3HT-based OSCs are summarized as follows:

(i) The use of P3HT as a donor is appropriate, as it has high thermal stability, suitable molecular properties, and good hole mobility. In terms of industrial aspect, the advantages of the lowest cost among all the donors, bulk availability, and excellent batch-to-batch purity make it a promising and distinct candidate;

(ii) Development of NFAs is the most important subject for the commercialization of P3HT-based OSCs. A question to be solved is how to obtain a compatible NFA particularly for P3HT. Here, we propose some guidelines:

(a) Rigid molecular backbone to avoid the energetic disorder within the molecule;
(b) Good solubility to ease the fabrication of uniform thin films. This chemical modification also correlates with the molecular packing in the blend film;
(c) Appropriate LUMO energy level of approximately -3.3 to -3.6 eV (matched with LUMO of P3HT ~2.8 eV) and minimum LUMO energy offset with proper electron transporting backbone is preferable to attain maximum V_{oc} and also reduce the energy loss;
(d) Semi-crystalline to amorphous nature. As P3HT has crystalline nature in the film after the thermal annealing, semi-crystalline to amorphous nature of NFAs should be anticipated to prevent the excess aggregation in the blend film;
(e) Comparable electron mobility with that of P3HT in the blend;
(f) Good miscibility with both P3HT and nonhalogenated green solvent.

These guidelines may be helpful for the further enhancement of the OSC performance, which leads to the accomplishment of a PCE of up to 15% in near future. Considering several factors such as efficiencies, stability, device fabrication, and cost for OSC commercialization, P3HT:NFA-based OSCs are remarkably promising.

Conflicts of interest

There are no conflicts to declare.

Acknowledgements

This work was supported by JSPS KAKENHI (20H02814, 20K21224, 20H05841, 20KK0123, and 20K15352), CREST (J205101030), NEDO, and "Dynamic Alliance for Open Innovation Bridging Human, Environmental and Materials" from The Ministry of Education, Culture, Sports, Science and Technology, Japan.

Notes and references

1 G. Li, R. Zhu and Y. Yang *Nat. Photonics*, 2012, **6**, 153-161.
2 L. Lu, T. Zheng, Q. Wu, A. M. Schneider, D. Zhao and L. Yu *Chem. Rev.*, 2015, **115**, 12666-12731.
3 L. Dou, J. You, Z. Hong, Z. Xu, G. Li, R. A. Street and Y. Yang, *Adv. Mater.*, 2013, **25**, 6642–6671.
4 F. F. Krebs, N. Espinosa, M. Hösel, R.R. Søndergaard and M. Jorgensen*, Adv. Mater.*, 2014, **26**, 29–39.
5 M. Hiramoto, H. Fujiwara and M. Yokoyama, *Appl. Phys. Lett.*, 1991, **58**, 1062–1064.
6 G. Yu, J. Gao, J. C. Hummenlen, F. Wudl and A. J. Heeger, *Science*, 1995, **270**, 1789–1791.
7 A. J. Heeger, *Adv. Mater.*, 2014, **26**, 10–28.
8 L. Meng, Y. Zhang, X. Wan, C. Li, X. Zhang, Y. Wang, X. Ke, Z. Xiao, L. Ding, R. Xia, H. L. Yip, Y. Cao and Y. Chen, *Science,* 2018, **361**, 1094–1098.
9 Y. Cui, H. Yao, J. Zhang, T. Zhang, Y. Wang, L. Hong, K. Xian, B. Xu, S. Zhang and J. Peng, *Nat. Commun.*, 2019, **10**, 2515 (1-8).
10 Y. Cui, H. Yao, J. Zhang, K. Xian, T. Zhang, L. Hong, Y. Wang, Y. Xu, K. Ma, C. An, C. He, Z. Wei, F. Gao and J. Hou, *Adv. Mater.*, 2020, **32**, 1908205 (1-7).
11 Q. Liu, Y. Jiang, K. Jin, J. Qin, J. Xu, W. Li, J. Xiong, J. Liu, Z. Xiao, K. Sun, S. Yang, X. Zhang and L. Ding, *Science Bulletin*, 2020, **65**, 272–275.
12 X. Du, T. Heumueller, W. Gruber, A. Classen, T. Unruh, N. Li and C. J. Brabec, *Joule*, 2019, **3**, 215–226.
13 W. R. Mateker, I. T. Sachs-Quintana, G. F. Burkhard, R. Cheacharoen and M. D. McGehee, *Chem. Mater.*, 2015, **27**, 404–407.
14 I. V. Martynov, A. V. Akkuratov, S. Y. Luchkin, S. A. Tsarev, S. D. Babenko, V. G. Petrov, K. J. Stevenson and P. A. Troshin, *ACS Appl. Mater. Interfaces*, 2019, **11**, 21741–21748.
15 S. A. Gevorgyan, N. Espinosa, L. Ciammaruchi, B. Roth, F. Livi, S. Tsopanidis, S. Zufle, S. Queiros, A. Gregori, G. A. D. Benatto, M. Corazza, M. V. Madsen, M. Hosel, M. J. Beliatis, T. T. Larsen-Olsen, F. Pastorelli, A. Castro, A. Mingorance, V. Lenzi, D. Fluhr, R. Roesch, M. M. D. Ramos, A. Savva, H. Hoppe, L. S. A. Marques, I. Burgues, E. Georgiou, L. Serrano-Lujan and F. C. Krebs, *Adv. Energy Mater.*, 2016, **6**, 1600910 (1-9).
16 *P.* R. Buseck, S. J. Tsipursky and R. Hettich, *Science*, 1992, **257**, 215–217.
17 J. C. Hummenlen, B. W. Night, F. LePeq, F. Wudl, J. Yao and C. L. Wilkins, *J. Org. Chem.*, 1995, **60**, 532–538.
18 B. C. Thompson and J. M. J. Fréchet, *Angew. Chem. Int. Ed.*, 2008, **47**, 58–77.
19 C. J. Brabec, S. Gowrisanker, J. J. M. Halls, D. Laird, S. Jia and S. P Williams, *Adv. Mater.*, 2010, **22**, 3839–3856.
20 L. Lu, T. Zheng, Q. Wu, A. M. Schneider, D. Zhao and L. Yu, *Chem. Rev.*, 2015, **115**, 12666–12731.

21 N. D. Treat, M. A. Brady, G. Smith, M. F. Toney, E. J. Kramer, C. J. Hawker and M. L. Chabinyc, *Adv. Energy Mater.*, 2011, **1**, 82–89.
22 W. Ma, J. R. Tumbleston, M. Wang, E. Gann, F. Huang and H. Ade, *Adv. Energy Mater.*, 2013, **3**, 864–872.
23 A. a. F. Eftaiha, J.-P. Sun, I. G. Hill and G. C. Welch, *J. Mater. Chem. A*, 2014, **2**, 1201–1213.
24 Y. Lin and X. Zhan, *Mater. Horiz.*, 2014, **1**, 470–488.
25 G. Zhang, J. Zhao, P. C. Y. Chow, K. Jiang, J. Zhang, Z. Zhu, J. Zhang, F. Huang and H. Yan, *Chem. Rev.*, 2018, **118**, 3447–3507.
26 W. Chen and Q. Zhang, *J. Mater. Chem. C*, 2017, **5**, 1275–1302.
27 W. Zhao, S. Li, H. Yao, S. Zhang, Y. Zhang, B. Yang and J. Hou, *J. Am. Chem. Soc.*, 2017, **139**, 7148–7158.
28 N. K. Elumalai and A. Uddin, *Energy Environ. Sci.*, 2016, **9**, 391–410.
29 G. E. Park, S, Choi, S. Y. Park, D. H. Lee, M. J. Cho and D. H. Choi, *Adv. Energy Mater.*, 2017, **7**, 1700566 (1–10).
30 S. Li, C-Z. Li, M. Shi and H. Chen, *ACS Energy Lett.*, 2020, **5**, 1554–1567.
31 H-L. Yip and A. K.-Y. Jen, *Energy Environ. Sci.*, 2012, **5**, 5994–6011.
32 F. C. Krebs, S. A. Gevorgyan and J. Alstrup, *J. Mater. Chem.*, 2009, **19**, 5442–5451.
33 D. A. Lyashenko, A. A. Zakhidov, V. A. Pozdin and G. G. Malliaras, *Org. Electron.*, 2010, **11**, 1507–1510.
34 M. Osaka, H. Benten, L-T. Lee, H. Ohkita and S. Ito, *Polymer*, 2013, **54**, 3443–3447.
35 J-F. Chang, B. Sun, D. W. Breiby, M. M. Nielsen, T. I. Solling, M. Giles, I. McCulloch and H. Sirringhaus, *Chem. Mater.*, 2004, **16**, 4772–4776.
36 F. Machui, S. Langner, X. Zhu, S. Abbott and C. J. Brabec, *Sol. Energy Mater. Sol. Cells,* 2012, **100**, 138–146.
37 H. Aarnio, P. Sehati, S. Braun, M. Nyman, M. P. de Jong, M. Fahlman and R. Österbacka, *Adv. Energy Mater.*, 2011, **1**, 792–797.
38 M. T. Dang, L. Hirsch and G. Wantz, *Adv. Mater.*, 2011, **23**, 3597–3602.
39 A. Wadsworth, Z. Hamid, M. Bidwell, R. S. Ashraf, J. I. Khan, D. H. Anjum, C. Cendra, J. Yan, E. Rezasoltani, A. A. Y. Guilbert, M. Azzouzi, N. Gasparini, J. H. Bannock, D. Baran, H. Wu, J. C. de Mello, C. J. Brabec, A. Salleo, J. Nelson, F. Laquai and I. McCulloch, *Adv. Energy Mater.*, 2018, **8**, 1801001 (1–15).
40 X. Li, F. Pan, C. Sun, M. Zhang, Z. Wang, J. Du, J. Wang, M. Xiao, L. Xue, Z.-G. Zhang, C. Zhang, F. Liu and Y. Li, *Nat. Commun.*, 2019, **10**, 519 (1–11).
41 R. Po, A. Bernardi, A. Calabrese, C. Carbonera, G. Corso and A. Pellegrino, *Energy Environ. Sci.,* 2014, **7**, 925−943.
42 Y. Jin, Z. Chen, M. Xiao, J. Peng, B. Fan, L. Ying, G. Zhang, X.-F. Jiang, Q. Yin, Z. Liang, F. Huang and Y. Cao, *Adv. Energy Mater.*, 2017, **7**, 1700944 (1–8).
43 R. D. McCullough, S. Tristram-Nagle, S. P. Williams, R. D. Lowe and M. Jayaraman, *J. Am. Chem. Soc.*, 1993, **115**, 4910−4911.
44 R. D. McCullough, *Adv. Mater.*, 1998, **10**, 93−116.
45 L. Ma, S. Zhang, J. Wang, Y. Xu and J. Hou, *Chem. Commun.*, 2020, **56**, 14337−14352.
46 J. H. Bannock, S. H. Krishnadasan, A. M. Nightingale, C. P. Yau, K. Khaw, D. Burkitt, J. J. M. Halls, M. Heeney and J. C. de Mello, *Adv. Funct. Mater.*, 2013, ***23***, 2123−2129.
47 N. Espinosa, M. Hosel, M. Jorgensen and F. C. Krebs, *Energy Environ. Sci.*, 2014, **7**, 855−866.
48 S. Strohm, F. Machui, S. Langner, P. Kubis, N. Gasparini, M. Salvador, I. McCulloch, H.-J. Egelhaaf and C. J. Brabec, *Energy Environ. Sci.*, 2018, **11**, 2225−2234.
49 M. Finn, C. J. Martens, A. V. Zaretski, B. Roth, R. R. Søndergaard, F. C. Krebs and D. J. Lipomi, *Sol. Energy Mater. Sol. Cells*, 2018, **174**, 7–15.
50 S. R. Dupont, M. Oliver, F. C. Krebs and R. H. Dauskardt, *Sol. Energy Mater. Sol. Cells*, 2012, **97**, 171–175.
51 M. Vilkman, K.-L. Väisänen, P. Apilo, R. Po, M. Välimäki, M. Ylikunnari, A. Bernardi, T. Pernu, G. Corso, J. Seitsonen, S. Heinilehto, J. Ruokolainen and J. Hast, *ACS Appl. Energy Mater.*, 2018, **1**, 5977–5985.
52 M. Zhang, X. Guo, W. Ma, H. Ade and J. Hou, *Adv. Mater.*, 2014, **26**, 5880–5885.
53 Y. Qin, M. A. Uddin, Y. Chen, B. Jang, K. Zhao, Z. Zheng, R. Yu. T. J. Shin, H. Y. Woo and J. Hou, *Adv. Mater.*, 2016, **28**, 9416–9422.
54 T. P. Kaloni, P. K. Giesbrecht, G. Schreckenbach and M. S. Freund, *Chem. Mater.* 2017, **29**, 10248–10283.
55 H. Fu, Z. Wang and Y. Sun, *Angew. Chem. Int. Ed.*, 2019, **58**, 4442–4453.
56 Q. Wang, Y. Qin, M. Li, L. Ye and Y. Geng Adv. Energy Mater., 2020, **10**, 2002572 (1–26).
57 M. Al Kobaisi, S. V. Bhosale, K. Latham, A. M. Raynor and S. V. Bhosale, *Chem. Rev.*, 2016, **116**, 11685–11796.
58 Z. Liu, G. Zhang and D. Zhang, *Acc. Chem. Res.*, 2018, **51**, 1422–1432.
59 G. Ren, E. Ahmed and S.A. Jenekhe, *Adv. Energy Mater.*, 2011, **1**, 946–953.
60 E. Ahmed, G. Ren, F. S. Kim, E. C. Hollenbeck and S.A. Jenekhe, *Chem. Mater.*, 2011, **23**, 4563–4577.
61 R. Fernando, Z. Mao and G. Sauvé, *Org. Electronics,* 2013, **14**, 1683–1692.
62 R. Fernando, Z. Mao, E. Muller, F. Ruan and G. Sauvé, *J. Phys. Chem. C,* 2014, **118**, 3433–3442.
63 D. Srivani, A. Gupta, D. D. La, R. S. Bhosale, A. L. Puyad, W. Xiang, J. Li, S. V. Bhosale and S. V. Bhosale, *Dyes and Pigments*, 2017, **53**, 7080–7083.
64 D. Srivani, A. Gupta, S. V. Bhosale, A. L. Puyad, W. Xiang, J. Li, R. A. Evans and S. V. Bhosale, *Chem. Commun.*, 2017, **53**, 7080–7083.
65 P. S. Rao, A. Gupta, D. Srivani, S. V. Bhosale, A. Bilic, J. Li, W. Xiang, R. A. Evans and S. V. Bhosale, *Chem. Commun.*, 2018, **54**, 5062–5065.
66 P. S. Rao, V. G. More, A. D. Jangale, S. V. Bhosale, R. S. Bhosale, A. L. Puyad, J-Y. Chen, J-L. Li, S. V. Bhsale, A. Gupta and G. D. Sharma, *Dyes and Pigments,* 2019, **171**, 107677.
67 V. Sharma, J. D. B. Koenig and G. C. Welch *J. Mater. Chem. A*, 2021, **9**, 6775–6789.
68 Y. Patil and R. Misra, *Chem. Rec.*, 2018, **18**, 1350–1364.
69 G. D. Sharma, M. S. Roy, J. A. Mikroyannidis and K. R. J. Thomas, *Org. Electron.*, 2012, **13**, 3118–3129.
70 Y. Ie, T. Sakurai, S. Jinnai, M. karakawa, K. Okuda, S. Mori and Y. Aso, *Chem. Commun.*, 2013, **49**, 8386–8388.
71 Q. Yan, Y. Zhou, Y-Q. Zheng, J. Pei and D. Zhao, *Chem. Sci.*, 2013, **4**, 4389–4394.
72 Z. Lu, X. Zhang, C. Zhan, B. Jiang, X. Zhang, L. Chen and J. Yao, *Phys. Chem. Chem. Phys.*, 2013, **15**, 11375–11385.
73 B. Jiang, X. Zhang, C. Zhan, Z. Lu, J. Huang, X. Ding, S. He and J. Yao, *Polym. Chem.*, 2013, **4**, 4631–4638.
74 X. Zhang, B. Jiang, X. Zhang, A. Tang, J. Huang, C. Zhan and J. Yao, *J. Phys. Chem. C*, *2014*, **118**, 24212–24220.
75 Y. Lin, J. Wang, S. Dai, Y. Li, D. Zhu and X. Zhan, *Adv. Energy Mater.*, 2014, **4**, 1400420.
76 Y. Zhang, Y. Xiao, Y. Xie, L. Zhu, D. Shi and C. Chen, *Org. Eletron.*, 2015, **21**, 184–191.
77 Y. Zhou, L. Ding, K. Shi, Y-Z. Dai, N. Ai, J. Wang and J. Pei, *Adv. Mater.*, 2012, **24**, 957–961.
78 Y-Q. Zheng, Y-Z. Dai, Y. Zhou, J-Y. Wang and J. Pei, *Chem. Commun.*, 2014, **50**, 1591–1594.

79 L. Ding, C-Y. Yang, Y-Q. Zheng, J-Y. Wang, J. Pei and Z. Su, *Asian J. Org. Chem.*, 2017, **6**, 1231–1234.
80 T. V. Pho, F. M. Toma, M. L. Chabinyc and F. Wudl, *Angew. Chem. Int. Ed.*, 2013, **52**, 1446–1451.
81 T. V. Pho, F. M. Toma, B. J. T.de Villers, S. wang, N. D. treat, N. D. Eisenmenger, G. M. Su, R. C. Coffin, J. D. Douglas, J. M. J. Frechet, G. C. Bazan, F. Wudl and M. L. Chabinyc, *Adv. Energy Mater.*, 2014, **4**, 1301007.
82 R-Q. Lu, Y-Q. Zheng, Y-N. Zhou, X-Y. Yan, T. Lei, K. Shi, Y. Zhou, J. Pei, L. Zoppi, K. K. Baldridge, J. S. Seigel and X-Y. Cao, *J. Mat. Chem. A*, 2014, **2**, 20515–20519.
83 K. N. Winzenberg, P. Kemppinen, F. H. Scholes, G. E. Collis, Y. Shu, Th. B. Sing, A. Bilic, C. M. Forsyth and S. E. Watkins, *Chem. Commun.*, 2013, **49**, 6307–6309.
84 A. M. Poe, A. M. D. Pelle, A. V. Subrahmanyam, W. White, G. Wantz and S. Thayumanavam, *Chem. Commun.*, 2014, **50**, 2913–2915.
85 Y. Kim, C. E. Song, S-J. Moon and E. Lim, *Chem. Commun.*, 2014, **50**, 8235–8238.
86 S. Holliday, R. S. Ashraf, C. B. Nielsen, M. Kirkus, J. A. Rohr, C-H. Tan, E. Collado-Fregoso, A-C. Knall, J. R. Durrant, J. Nelson and I. McCulloch, *J. Am. Chem. Soc.*, 2015, **137**, 898–904.
87 H. Shi, W. M. Shi, J. Ling and H. Chen, *J. Mater. Chem. A*, 2015, **3**, 1902–1905.
88 S. Li, J. Yan, C-Z. Li, F. Liu. M. Shi, H. Chen and T. P. Russell, *J. Mater. Chem. A*, 2016, **4**, 3777–3783.
89 Y. Lin, Y. Li and X. Zhan, *Adv. Energy Mater.*, 2013, **3**, 724–728.
90 A. M. Raynor, A. Gupta, H. Patil, D. Ma, A. Bilic, T. J. Rook and S. V. Bhosale, *RSC Adv.*, 2016, **6**, 28103–28109.
91 T. T. Do, K. Rundel, Q. Gu, E. Gann, S. manzhos, K. Feron, J. bell, C. R. Mcneill and P. Sonar, *New J. Chem.*, 2017, **41**, 2899–2909.
92 T. T. Do, H. D. Pham, S. Manzhos, J. M. Bell and P. Sonar, *ACS Appl. Mater. Interfaces*, 2017, **9**, 16967–16976.
93 Y. Wu, H. Bai, Z. Wang, P. Cheng, S. Zhu, Y. Wang, W. Ma and X. Zhan, *Energy Environ. Sci.*, 2015, **8**, 3215–3221.
94 Q. He, T. Li, C. Yan, Y. Liu, J. Wang, M. Wang, Y. Lin and X. Zhan, *Dyes and Pigments*, 2016, **128**, 226–234.
95 S. Holliday, R. S. Ashraf, A. Wadsworth, D. Baran, S. A. Yousaf, C. B. Nielsen, C-H. Tan,S. D. Dimitrov, Z. Shang, N. Gasparini, M. Alamoudi, F. Laquai, C. J. Brabec, A. Salleo, J. R. Durrant and I. McCulloch, *Nat. Commun.*, 2016, **7**, 11585–11595.
96 D. Baran, R. S. Ashraf, D. A. Hanifi, M. Abdelsamie, N. Gasparini, J. A. Rohr, S. Holliday, A. Wardsworth, S. Lockett, M. Neophytou, C. J. M. Emmott, J. Nelson, C. J. Brabec, A. Amassian, A. Salleo, T. Kirchartz, J. R. Durrant and I. McCulloch, *Nat. Mater.*, 2017, **16**, 363–369.
97 B. Xiao, A. Tang, J. Zhang, A. Mahmood, Z. Wei and E. Zhou, *Adv. Energy Mater.*, 2017, **7**, 1602269.
98 B. Xiao, A. Tang, J. Yang, Z. Wei and E. Zhou, *ACS Macro Lett.*, 2017, **6**, 410–414.
99 B. Xiao, A. Tang, L. Cheng, J. Zhang, Z. Wei, Q. Zeng and E. Zhou *Sol. RRL*, 2017, **1**, 1700166.
100 B. Xiao, A. Tang, Q. Zhang, G. Li, X. Wang and E. Zhou, *ACS Appl. Mater. Interfaces*, 2018, **10**, 34427–34434.
101 Q. Zhang, B. Xiao, M. Du, G. Li, A. Tang and E. Zhou, *J. Mater. Chem. C*, 2018, **6**, 10902–10909.
102 B. Xiao, A. Tang, J. Yang, A. Mahmood, X. Sun and E. Zhou, *ACS Appl. Mater. Interfaces*, 2018, **10**, 10254–10261.
103 B. Xiao, Q. Zhang, G. Li, M. Du, Y. Geng, X. Sun, A. Tang, Q. Guo and E. Zhou, *Sci. China. Chem.*, 2020, **63**, 254–264.
104 C. Xiao, M. Du, X. Wang, Z. Xiao, G. Li, A. Tang, L. Ding, Y. Geng, X. Sun and E. Zhou, *ACS Appl. Mater. Interfaces*, 2020, **12**, 1094–1102.
105 X. Wang, A. Tang, J. Yang, M. Du, J. Li, G. Li, Q. Guo and E. Zhou, *Sci. China. Chem.*, 2020, **63**, 1666–1174.
106 J. Wang, T. Li, X. Wang, Y. Xiao, C. Zhong, J. Wang, K. Liu, X. Lu, X. Zhan and X. Chen, *ACS Appl. Mater. Interfaces*, 2019, **11**, 26005–26016.
107 J. Wang, G. Cai, B. Jia, H. Lu, X. Lu, X. Zhan and X. Chen, *J. Mater. Chem. A*, 2021, **9**, 6520–6528.
108 H. Huang, B. Xiao, C. Huang, J. Zhang, S. Liu, N. Fu, B. Zhao, T. Qin, E. Zhou and H. Huang, *J. Mater. Chem. C*, 2018, **6**, 12347–12354.
109 P. Ye, Y. Chen, J. Wu, X. Wu, Y. Xu, Z. Li, S. Hong, M. Sun, A. Peng and H. Huang, *Mater. Chem. Front.*, 2019, **3**, 64–69.
110 J. Wu, Y. Xu, Z. Yang, Y. Chen, X. Sui, L. Yang, P. ye, T. Zhu, X. Wu, X. Liu, H. Cao, A. Peng and H. Huang, *Adv. Energy Mater.*, 2019, **9**, 1803012.
111 T. Li, J. Wang, H. Chen, P. Chen, S. Huang, Y. Lin, H. Yu and X. Zhan, *Dyes and Pigments*, 2017, **137**, 553–559.
112 T. R. Andersen, A. T. Weyhe, Q. Tao, F. Zhao, R. Qin, S. Zhang, H. Chen and D. Yu, *Mater. Adv*., 2020, **1**, 658–665.
113 J. T. Bloking, X. Han, A. T. Higgs, J. P. Kastrop, L. Pandey, J. E. Norton, C. Risko, C. E. Chwn, J-L. Bredas, M. D. McGehee and A. Sellinger, *Chem. Mater.*, 2011, **23**, 5484–5490.
114 N. C. Giebink , G. P. Wiederrecht , M. R. Wasielewski and S. R. Forrest, *Phys. Rev. B*, 2011 , **83** , 195326.
115 Y. fang, A. K. Pandey, A. M. Nardes, N. Kopidakis, P. L. Burn and P. Meredith, *Adv. Energy Mater.*, 2013, **3**, 54–59.
116 Y. Ie. S. Jinnai, M. Nitani and Y. Aso, *J. Mater. Chem. C*, 2013, **1**, 5373–5380.
117 S. Jinnai, Y. Ie, M. karakawa, T. Aernouts, Y. Nakajima, S. Mori and Y. Aso, *Chem. Mater.*, 2016, **28**, 1705–1713.
118 J. Ahn, S. Oh, H. Lee, S. Lee, C. E. Song, H. K. Lee, S. K. Lee, W-W. So, S-J. Moon, E. Lim, W. S. Shin and J-C. Lee, *ACS Appl. Mater. Interfaces*, 2019, **11**, 30098–30107.
119 S. Chatterjee, Y. Ie andY. Aso, *J. Photopolym. Sci. Technol.*, 2017, **30**, 557–560.
120 S. Chatterjee, Y. Ie, M. Karakawa and Y. Aso, *Adv. Funct. Mater.*, 2016, **26**, 1161–1168.
121 S. Chatterjee, Y. Ie and Y. Aso, *ACS Omega*, 2018, **3**, 5814–5824.
122 S. Jinnai and Y. Ie, *J. Photopolym. Sci. Technol.*, 2021 (Accepted).
123 S. Chatterjee, Y. Ie, T. Seo, T. Moriyama, Gert-Jan. A. H. Wetzelaer, P. W. M. Blom and Y. Aso, *NPS Asia Mater.*, 2018, **10**, 1016–1028.
124 Y. Cui, H. Yao, L. Hong, T. Zhang, Y. Tang, B. Lin, K. Xian, B. Gao, C. An, P. Bi, W. Ma and J. Hou, *Natl. Sci. Rev.* 2020, **7**, 1239–1246.
125 C. Yang, S. Zhang, J. Ren, M. Gao, P. Bi, L. Ye and J. Hou, *Energy Environ. Sci.*, 2020, **13**, 2864–2869.
126 C. Yang, R. Yu, C. Liu, H. Li, S. Zhang and J. Hou, *ChemSusChem*, DOI: 10.1002/cssc.202100627.
127 J. Yang, Y. Geng, J. Li, B. Zhao, Q. Guo and E. Zhou, *J Phys. Chem. C*, 2020, **124**,24616–24623.
128 P. Sonar, G-M. Ng, T. T. Lin, A. Dodabalapur and Z-K. Chen, *J. Mater. Chem.,* 2010, **20**, 3626–3636.
129 P. Josse, C. Dalinot, Y. Jiang, S. Dabos-Seignon, J. Roncali, P. Blanchars and C. Cabanetos *J. Mater. Chem. A*, 2016, **3**, 250–256.
130 Z. Zhang, W. Liu, J. Yan, M. Shi and H. Chen, *Synth. Met.*, 2016, **222**, 211–218.
131 M. Privado, V. Cuesta, P. de la Cruz, M. L. Khestov, R. Singhal, G. D. Sharma and F. Langa, *ACS Appl. Mater. Interfaces*, 2017, **9**, 11739–11748.
132 P. Josse, P. Chavez, C. Dindault, C. Dalinot, S. M. McAfee, S. Dabos-Seignon, D. Tondelier, G. Welch, P. Vlanchard, N. Leclerc and X. Cabanetos, *Dyes and Pigments*, 2017, **137**, 576–583.
133 Z. Mao, W. Senevirathna, J-Y. Liao, J. Gu, S. V. Kesava, C. Guo, E. D. Gomez and G. Sauvé, *Adv. Mater.*, 2014, **26**, 6290–6294.

134 S. Pejic, A. M. Thomsen, F. S. Etheridge, R. Fernando, C. Wang and G. Sauvé *J. Mater. Chem. C*, 2018, **6**, 3990–3998.
135 C. Wang, P. Wei, J. H. L. Ngai, A. L. Rheingold, T. G. Gray, Y. Li, E. Pentzer, R. Li, L. Zhu and G. Sauvé, *J. Mater. Chem. A* 2019, **7**, 24614–24625.
136 C. Wang, M. Zhao, A. L. Rheingold and G. Sauvé, *J. Phys. Chem. C*, 2020, **124**, 8541–8549.
137 Y. Yang, G. Zhang, C. Yu, C. He, J. Wang, X. Chen, J. Yao, Z. Liu and D. Zhang, *Chem. Commun.*, 2014, **50**, 9939–9942.
138 X-F. Wu, W-F. Fu, Z. Xu, M. Shi, F. Liu, H-Z. Chen, J-H. Wan and T. P. Russell, *Adv. Funct. Mater.*, 2015, **25**, 5954–5966.
139 N. Qiu, X. Yang, H. Zhang, X. Wang, C. Li, F. Liu, H. Zhang, T. P. Russell and Y. Chen, *Chem. Mater.*, 2016, **28**, 6770–6778.
140 S. Li, W. Liu, M. Shi, J. Mai, T-K, Lau, J. Wan, X. Lu, C-Z. Li and H. Chen, *Energy Environ. Sci.*, 2016, **9**, 604–610.
141 W. Liu, S. Li, J. Huang, S. yang, J. Chen, L. Zuo, M. Shi, X. Zhan, C-Z. Li and H. Chen, *Adv. Mater.*, 2016, **28**, 9729–9734
142 C. Yuan, W. Liu, M. Shi, S. Li, Y. Wang, H. Chen, C-Z. Li and H. Chen, Dyes and *Pigments*, 2017, **143**, 217–222.
143 A. K. Hundal, S. Ali, M. Jameel, L. Jones, N. Kaur, R. A. Evans, J-L. Li, S. J. Langford and A. Gupta, *Mater. Chem. Front.*, 2020, **4**, 3209–3215.
144 Y. Lin, P. Cheng, Y. Li and X. Zhan, *Chem. Commun.*, 2012, **48**, 4773–4775.
145 X. Liu, Y. Xie, H. Zhao, X. Cai, H. Wu, S-J. Su and Y. Cao, *New J. Chem.*, 2015, **39**, 8771–8779.
146 A. Rananaware, A. Gupta, J. Li, A. Bilic, L. Jones, S. Bhargava and S. V. Bhosale, *Chem. Commun*., 2016, **52**, 8522–8525.
147 A. Rananaware, A. Gupta, G. Kadam, D. D. La, A. Bilic, W. Xiang, R. A. Evans and S. V. Bhosale, *Mater. Chem. Front.*, 2017, **1**, 2511–2518.
148 S. M. Wagalgave, S. V. Bhosale, R. S. Bhosale, A. L. Puyad, J-Y. Chen, J-L. Li, R. C. Evans, A. Gupta and S. V. Bhosale, *Mater. Chem. Front.*, 2019, **3**, 1231–1237.
149 X. Xu, G. Zhang, L. Yu, R. Li and Q. Peng *Adv. Mater.*, 2019, **31**, 1906045.
150 F. G. Brunetti, X. Gong, M. Tong, A. J. Heeger and F. Wudl, *Angew. Chem. Int. Ed.*, 2010, **49**, 532–536.
151 X. Gong, M. Tong, F. G. Brunetti, J. Seo, Y. Sun, D. Moses, F. Wudl and A. J. Heeger, *Adv. Mater.*, 2011, **23**, 2272–2277.
152 Y. Shu, Y-F. Lim, Z. Li, B. Purushothaman, R. Hallani, J. E. Kim, S. R. Parkin, G. G. Malliaras and J. E. Anthony, *Chem. Sci.* 2011, **2**, 363–368.
153 T. Zhou, T. Jia, B. kang, F. Li, M. Fahlman and Y. Wang, *Adv. Energy Mater.*, 2011, **1**, 431–439.
154 O. K. Kwon, J-H. Park, S. K. Park and S. Y. Park, *Adv. Energy Mater.*, 2015, **5**, 1400929.
155 H-Y. Chen, J. Golder, S-C. Yeh, C-W. Lin, C-T. Chen, C-T. Chen *RSC Adv.* 2015, **5**, 3381-3385.
156 P. Chandra Kanth, J. Patel, M. Chauhan, M. Aatif, A. Sharma, M. U. Trivedi, B. Tripathi, J. P. Tiwari, G. Gupta, M. Kumar and M. K. Pandey, *New J. Chem.*, 2017, **41**, 5836–5845.
157 M. Zhu, J. Miao, Z. Hu, Y. Chen, M. Liu, I. Murtaza and H. Meng, *Dyes and Pigments*, 2017, **142**, 39–50.
158 Y. Wang, B. Kan, X. Ke, F. Liu, X. Wan, H. Zhang, C. Li and Y. Chen, *Sol. RRL*, 2018, **2**, 1700179.
159 Y. Li, X. Liu, F-P. Wu, Y. Zhou, Z-Q. Jiang, B. Song, Y. Xia, Z-G. Zhang, F. Gao, O. Inganas, Y. F. Li and L-S. Liao, *J. Mater. Chem. A.*, 2016, **4**, 5890–5897.
160 X. Liu, Y. Li, P. Huang, Y. Zhou, Z-Q. Jiang, B. Song, Y. Li, L-S. Liao and Y. Zheng, *J. Power Sources,* 2017, **364**, 426–431.
161 T. M. Grant, K. L. C. Kaller, T. J. Coathup, N. A. Rice and K. Hinzer, *Org. Electron.*, 2020, **87**, 105976 (1-8).
162 H. Liu, W. Wang, Y. Zhou and Z. Li *J. Mater. Chem. A*, 2021, **9**, 1080–1088.
163 J. J. M. Halls, C. A. Walsh, N. C. Greenham, E. A. Marseglia, R. H. Friend, S. C. Moratti and A. B. Holmes, *Nature*, 1995, **376**, 498.
164 J. Yang, B. Xiao, A. Tang, J. Li, X. Wang, E. Zhou, *Adv. Mater.* 2019, **31**, 1804699.
165 K. D. Deshmukh, T. Qin, J. K. Gallaher, A. C. Y. Liu, E. Gann, K. O'Donnell, L. Thomsen, J. M. Hodgkiss, S. E. Watkins and C. R. McNeill, *Energy Environ. Sci.*, 2015, **8**, 332–342.
166 B. Fan, L. Ying, P. Zhu, F. Pan, F. Liu, J. Chen, F. Huang, and Y. Cao, *Adv. Mater.*, 2017, **29**, 1703906.
167 Z. Li, L. Ying, P. Zhu, W. Zhong, N. Li, F. Liu, F. Huang and Y. Cao, *Energy Environ. Sci.*, 2019, **12**, 157–163.
168 Z.-G. Zhang, Y. Yang, J. Yao, L. Xue, S. Chen, X. Li, W. Morrison, C. Yang and Y. Li, *Angew. Chem. Int. Ed.*, 2017, **56**, 13503–13507.
169 H. Benten, D. Mori, H. Ohkita and S. Ito, *J. Mater. Chem. A*, 2016, **4**, 5340–5365.
170 C. Lee, S. Lee, G.-U. Kim, W. Lee and B. J. Kim, *Chem. Rev.*, 2019, **119**, 8028–8086.
171 G. Wang, F. S. Melkonyan, A. Facchetti and T. J. Marks, *Angew. Chem. Int. Ed.*, 2019, **58**, 4129–4142.
172 N. Zhou and A. Facchetti, *Mater. Today*, 2018, **21**, 377–390.
173 Q. Shi, J. Wu, X. Wu, A. Peng and H. Huang, *Chem. Eur. J.*, 2020, **26**, 12510–12522.
174 C. R. McNeill, A. Abrusci, J. Zaumseil, R. Wilson, M. J. McKieman, J. H. Burroughes, J. J. M. Halls, N. C. Greenham and R. H. Friend, *Appl. Phys. Lett.*, 2007, **90**, 193506.
175 X. He, F. Gao, G. Tu, D. Hasko, S. Hüttner, U. Steiner, N. C. Greenham, R. H. Friend and W. T. S. Huck, *Nano Lett.*, 2010, **10**, 1302–1307.
176 W. Yu, D. Yang, X. Zhu, X. Wang, G. Tu, D. Fan, J. Zhang and C. Li, *ACS Appl. Mater. Interfaces*, 2014, **6**, 2350–2355.
177 Q. Yang, H. Song, B. Gao, Y. Wang, Y. Fu, J. Yang, Z. Xie and L. Wang, *RSC Adv*., 2014, **4**, 12579–12585.
178 D. Mori, H. Benten, J. Kosaka, H. Ohkita, S. Ito and K. Miyake, *ACS Appl. Mater. Interfaces*, 2011, **3**, 2924–2927.
179 D. Mori, H. Benten, H. Ohkita, S. Ito and K. Miyake, *ACS Appl. Mater. Interfaces*, 2012, **4**, 3325–3329.
180 M. Osaka, D. Mori, H. Benten, H. Ogawa, H. Ohkita, S. Ito *ACS Appl. Mater. Interfaces*, 2017, **9**, 15615–15622.
181 H. Yan, Z. Chen, Y. Zheng, C. Newman, J. R. Quinn, F. Dötz, M. Kastler and A. Facchetti, *Nature*, 2009, **457**, 679–686.
182 X. Zhan, Z. Tan, B. Domercq, Z. An, X. Zhang, S. Barlow, Y. Li, D. Zhu, B. Kippelen and S. R. Marder, *J. Am. Chem. Soc.*, 2007, **129**,7246–7247.
183 R. Steyrleuthner, M. Schubert, F. Jaiser, J. C. Blakesley, Z. Chen, A. Facchetti, D. Neher, *Adv. Mater.* 2010, **22**, 2799–2803.
184 J. R. Moore, S. Albert, A. Rao, S. Massip, B. Watts, D. J. Morgan, R. H. Friend, R. M. Christopher and H. Sirringhaus, *Adv. Energy Mater.*, 2011, **1**, 230–240.
185 S. Fabiano, Z. Chen, S. Vahedi, A. Facchetti, B. Pignataro and M. A. Loi, *J. Mater. Chem.*, 2011, **21**, 5891–5896.
186 H. Yan, B. A. Collins, E. Gann, C. Wang, H. Ade and C. R. McNeill, ACS Nano, 2012, **6**, 677–688.
187 M. Schubert, D. Dolfen, J. Frisch, S. Roland, R. Steyrleuthner, B. Stiller, Z. Chen, U. Scherf, N. Koch, A. Facchetti and D. Neher, *Adv. Energy Mater.*, 2012, **2**, 369–380.
188 S. Fabiano, S. Himmelberger, M. Drees, Z. Chen, R. M. Altamimi, A. Salleo, M. A. Loi and A. Facchetti, *Adv. Energy Mater.*, 2014, **4**, 1301409.
189 Y-J. Hwang, G. Ren, N. M. Murari and S. S. Jenekhe, *Macromolecules*, 2012, **45**, 9056–9062.
190 K. Nakabayashi and H. Mori, *Macromolecules* 2012, **45**, 9618–9625.
191 M. Yuan, M. M. Durban, P. D. Kazarinoff, D. F. Zeigler, A. H. Rice, Y. Segawa and C. K. Luscombe, *J. Polym. Sci. A*, 2013, **51**, 4061–4069.
192 E. Zhou, J. Cong, M. Zhao, L. Zhang, K. Hashimoto and K. Tajima, *Chem. Commun.,* 2012, **48**, 5283–5285.

193 S. Dai, P. Cheng, Y. Lin, Y. Wang, L. Ma, Q. Ling and X. Zhan, *Polym. Chem.*, 2015, **6**, 5254–5263.
194 S-C. Chen, Q. Zheng, Q. Zhang, D. Cai, J. Wang, Z. Yin and C. Tang, *J. Polym. Sci. A*, 2013, **51**, 1999–2005.
195 Y. Zhou, Q. Yan, Y-Q. Zheng, J-Y Wang, D. Zhao and J. Pei, , *J. Mater. Chem. A*, 2013, **1**, 6609–6613.
196 W. Liu, R. Tkachov, H. Komber, V. Senkovskyy, M. Schubert, Z. Wei, A. Facchetti, D. Neher and A. Kiriy, *Polym. Chem.*, 2014, **5**, 3404–3411.
197 C.-W. Ge, C.-Y. Mei, J. Ling, J.-T. Wang, F.-G. Zhao, L. Liang, H.-J. Li, Y.-S. Xie and W.-S. Li, *J. Polym. Sci. Part A*, 2014, **52**, 1200–1215.
198 I. H. Jung, W-Y. Lo, J. Jang, W. Chen, D. Zhao, E. S. Landry, L. Lu, D. V. Talapin and L. Yu, *Chem. Mater.*, 2014, **26**, 3450–3459.
199 W. Li, Y. An, M. M. Wienk and R. A. J. Janssen, *J. Mater. Chem. A*, 2015, **3**, 6756–6760.
200 X. Long, Z. Ding, C. Dou, J. Liu and L. Wang, *Mater. Chem. Front.* 2017, **1**, 852–858.
201 Y. Ie, K. Izuno, T. Moriyama and Y. Aso, *J. Photopolym. Sci. Technol.*, 2019, **32**, 721–725.
202 S. Zhang, L. Ye, H. Zhang and J. Hou, *Mater. Today*, 2016, **19**, 533–543.
203 J. Ma, B. Jhao, Y. Gong, J. Deng and Z. Tan *J. Mater. Chem. A*, 2019, **7**, 24826–22847.
204 Y. F. Lim, Y. Shu, S. R. Parkin, J. E. Anthony and G. G. Malliaras, *J Mat. Chem.* 2009, **19**, 3049–3056.
205 S. Chatterjee, T. Ohto, H. Tada, S. Jinnai and Y. Ie, *ACS Sustainable Chem. Eng.*, 2020, **8**, 19013–19022.
206 M. Hösel, R. R. Søndergaard, M. Jørgensen and F. C. Krebs, *Energy Technol*., 2013, **1**, 102–107.
207 G. Wang, M. A. Adil, J. Zhang and Z. Wei, *Adv. Mater*., 2019, **31**, 1805089 (1-34).
208 F. C. Krebs, T. Tromholt and M. Jørgensen, *Nanoscale* 2010, **2**, 873–886.
209 E. Bundgaard, O. Hagemann, M. Manceau, M. Jørgensen and F. C. Krebs, *Macromolecules* 2010, **43**, 8115–8120.